Magee Womens Research Institute and Foundation

Annual Progress Report: 2009 Formula Grant

Reporting Period

January 1, 2010 – June 30, 2010

Formula Grant Overview

The Magee Womens Research Institute and Foundation received $1,541,095 in formula funds for the grant award period January 1, 2010, through December 31, 2010. Accomplishments for the reporting period are described below.

Research Project 1: Project Title and Purpose

Refinement of the Appropriate Animal Model for Respiratory Infection with Influenza in Pregnancy - The purpose of the project is to develop and test a ferret model for respiratory challenge with influenza virus infection during pregnancy. This is critical given the disproportionate morbidity and mortality seen among pregnant women during previous influenza pandemics, seasonal epidemics and the current novel 2009 H1N1 influenza pandemic. Development of a pregnant animal model for respiratory challenge will also allow for future investigations to delineate more effectively the susceptibility to infection noted among pregnant women and their immunological response mechanisms. In addition, with the growing threat of bioterrorism and the fact that most category a bioterror agents would be targeted for inhalational spread, development of pregnant animal models allows for ongoing countermeasures' research against these agents in this unique population.

Anticipated Duration of Project

1/1/2010 - 12/31/2010

Project Overview

1. Further develop and refine a model of collaboration and infrastructure that will allow for ongoing investigation of susceptibility, immunological response and countermeasures to emerging and threatening infectious diseases among pregnant animals.
2. To demonstrate and compare the disease course of aerosolized novel 2009 H1N1 in both a late gestation pregnant and non-pregnant ferret model of influenza infection.
3. To evaluate and compare the pathogenesis and immune response elicited by aerosolized novel 2009 H1N1 in both late gestation pregnant and non-pregnant ferrets.

We will begin by examining aerosol characteristics of novel 2009 H1N1 influenza at 3 dilutions in an empty aerosol chamber starting at 10^8/ml and decreasing ten-fold. Four aerosols per dilution (12 aerosols) will be used in a whole-body exposure box and will then be repeated once

for validation. Subsequent determinations of viral concentration in the nebulizer and aerosol by Tissue Culture ID50 (TCID50) will be undertaken. After these quality and quantity control measures, challenge experiments will then be undertaken. Ferrets obtained from Marshall Pet Products will be used for the experiments. In order to determine the Infective Dose of 2009 H1N1 that establishes infection in 50% of ferrets (IC_{50}), aerosol challenges with 3 doses in a whole-body chamber at doses expected to bracket the IC_{50} will be performed upon 3 groups of four. Fifty percent of ferrets will be pregnant and 50% non-pregnant. Challenges will be performed on or about day 33 of a 42 day gestation, approximating 3rd trimester exposure. All ferrets will be followed for 10-14 days after exposure to document clinical disease course and to quantify upper respiratory tract viral load (PCR). Ferrets that become moribund will be promptly euthanized and necropsied; blood and tissue samples will be taken for analysis. Subsequently, challenges using the determined IC_{50} from the above aim will be performed among a second group of ferrets with four in each group (pregnant and non-pregnant, total N=8). The first group will undergo a sham challenge for control purposes. The next 3 groups will be challenged and then euthanized at days 2, 4 and 7 post-challenge. Pre-euthanization analysis will include: Viral load, Hemagluttin and microneutralization antibody titers, and potentially microarray technologies pending funding specifics. Post-euthanization analysis will include both pathologic and viral load quantification of tissue specimens, including the fetal compartment.

Principal Investigator

Richard H. Beigi, MD, MSc
Assistant Professor of Reproductive Sciences
Magee-Womens Hospital of UPMC
300 Halket Street
Department of OB/GYN/RS
Pittsburgh, PA 15213

Other Participating Researchers

Kelly Stefano-Cole, PhD, Doug Reed, PhD, Amy Hartman, PhD - employed by University of Pittsburgh, Center for Vaccine Research

Expected Research Outcomes and Benefits

We expect to develop a model for exposing ferrets to respiratory challenge with novel 2009 H1N1 influenza. This will allow for comparisons between pregnant and non-pregnant ferrets which is a unique component of this project. The understanding of pregnant women's increased severity of illness from influenza is not completely understood and was readily apparent during the current influenza pandemic. By performing these projects a relevant disease model will be developed to test various influenza strains of varying potency (including various pandemic strains). This model will also allow for a working collaboration for testing pregnant animals for other respiratory pathogens of high bio-security importance (such as anthrax, smallpox, plague, etc.). This is to our knowledge the only investigations into the pregnancy-specific characteristics of these threatening diseases, and having a relevant animal model will allow us to form a basis for future funded research studies potentially using non-human primates.

Eventually, components of what we learn and test will have human relevance in terms of pregnant women's response to such infections. It may also lead to potential ways to prevent disease through vaccination and to treat such infections in pregnant women. It is important to note that pregnant women are an often forgotten population in terms of research in this area yet are a crucially important sector of the population for many reasons. This research has potentially far reaching implications for societal benefit and protection, as this project represents concrete steps in strengthening this important collaboration between investigators and in developing this animal model on which to build.

Summary of Research Completed

At this point we have just recently obtained The Institutional Animal Care and Use Committee approval (IACUC #1007568) for our projects and will begin the viral challenges in August and September, 2010, to be carried out through the fall of 2010. Thus, we currently have no data to report.

Research Project 2: Project Title and Purpose

Relationships among PPAR gamma Activity, Hypoxia, and Differentiation in Human Placenta - The main purpose of this study is to understand the relations among four important biological processes occurring in human placenta: placental hypoxia, normal trophoblast differentiation, peroxisome proliferator-activated receptors (PPAR) gamma activity, and fetal growth restriction. By applying various statistical procedures to both historic and recently generated data sets, the results of this study could deepen our understanding of these placental processes from the genomic point of view, shed light on the mechanism behind the fetal growth restriction caused by hypoxic injury, and eventually facilitate the development of prevention and treatment methods for fetal growth restriction.

Anticipated Duration of Project

1/1/2010 - 12/31/2010

Project Overview

Fetal growth restriction (FGR) has been shown to result in fetal morbidity and mortality, as well as later health complications for adult survivors. One of the main risk factors of FGR is believed to be hypoxia, which may prevent trophoblast differentiation, enhance trophoblast apoptosis, and hence contribute to fetal growth restriction.

Peroxisome proliferator-activated receptors (PPAR) gamma is a transcription factor playing an important role in placental development and function. On one hand, a mouse model study shows that a PPAR gamma null murine placenta fails to terminally differentiate and is not permeated with fetal vessels; yet on the other hand, an in vitro study shows that PPAR gamma ligand troglitazone modulates trophoblast differentiation and attenuates trophoblast apoptosis under hypoxia condition.

Given the close relations among hypoxia, fetal growth restriction, trophoblast differentiation, and PPAR gamma activity, it is natural to ask if there are sets of genes whose expression patterns could explain both the close relationships and the dissimilarities among these processes. Moreover, assuming the pivotal role of hypoxia in FGR, it would also be interesting to know if there is a specific course of hypoxia during later stages of gestation that is responsible for most of the observed fetal growth restriction.

To answer these questions, in this project, I will conduct an exploratory study of the relationships among the transcriptomes of undifferentiated trophoblast, differentiated trophoblast (under normal condition), trophoblast under hypoxia, and trophoblast treated with PPAR ligands, as well as placentas from normal and FGR pregnancies. Both supervised and unsupervised statistical learning procedures will be employed. The data of this study include historical microarray gene expression data for primary trophoblast cell samples that are allowed to differentiation under normal condition, or treated with hypoxia, or treated with PPAR gamma ligands, as well as microarray data for both normal and FGR placenta. The microarray data are supplemented by recently generated qPCR data of 24 selected genes for normal and FGR placentas, and trophoblast cells treated under various hypoxia schemes.

Principal Investigator

Tianjiao Chu, PhD
Assistant Professor
University of Pittsburgh
204 Craft Ave., B409
Pittsburgh, PA 15213

Other Participating Researchers

Yoel Sadovsky, MD - employed by University of Pittsburgh

Expected Research Outcomes and Benefits

Through the exploratory study of the relationships among trophoblast differentiation, hypoxia, PPAR activity, and fetal growth restriction, this study should be able to identify both the sets of genes whose expression patterns may reveal both the connection and dissimilarity among hypoxia, trophoblast differentiation, PPAR gamma activity, and fetal growth restriction, and the genomic functional groups overrepresented in each set of these genes.

Moreover, by analyzing the qPCR data of the expression levels of a selected set of 24 genes in both in vivo conditions and in vitro conditions, this study could enable us to identify a specific course of hypoxia that is most likely responsible for the fetal growth restriction.

Ultimately, the results of this study will improve our understanding of the mechanism of hypoxic injury to placenta and the role PPAR gamma activity in regulating placental development and

provide insight on the connection between hypoxia and fetal growth restriction, therefore aiding in the prevention and treatment of fetal growth restriction.

Summary of Research Completed

Six month report:

In the first 6 month of this project, we studied the relations among primary trophoblast cells treated with different patterns of hypoxic conditions, primary trophoblast cell cultured at different normoxic conditions, as well as normal placentas and placentas from pregnancies with fetal growth restriction (FGR).

Data:
34 genes were selected from a previous microarray study of the gene expression level in normal placenta and FGR placentas, with 17 of them up-regulated in FGR placenta compared to the normal placenta, and 17 of them down-regulated in FGR placenta. Primary trophoblast cells, harvested from 5 normal placentas, were cultured with 12 different hypoxic/normoxic conditions (see Figure 1). In addition, 4 normal placentas and 4 FGR placenta samples were collected. Expression levels of the 34 genes were measured using qPCR for the 8 placenta samples as well as the primary human trophoblast (PHT) cell treated under 12 different conditions.

Supervised Analysis:
The main purpose of supervised analysis is to determine under which hypoxic/normoxic condition the PHT sample best mimics the FGR placenta by the comparison of gene expression profiles of the PHT samples under the 12 hypoxic/normoxic conditions to that of the normal and FGR placentas.

Linear Mixed Effect Models:
First, linear mixed effect models were used to identify, among all the 34 genes, if any of them are differentially expressed between normal placenta and FGR placenta. After adjusting the p-values to control the false discovery rate (FDR), none of these genes are significantly differentially expressed when FDR is controlled at 5%, but the following 3 genes: ABP1, FLRG, and PAPPA2 are significantly differentially expressed between normal and FGR placentas when FDR is controlled at 10%.

Logistic Regression:
Next, we used logistic regression methods to determine, among all the 12 hypoxic/normoxic conditions, which of them has an expression profile closest to the FGR placenta, and which of them has an expression profile closest to the normal placenta. For this purpose, we fit 34 logistic regression models for the normal and FGR placenta, where in each model, the response variable is a binary variable indicating whether a sample is FGR or normal, and the single predictor is the expression level of one of the 34 genes. We then used these 34 models to predict, for each PHT sample under each condition, the probability that this sample can be classified as normal placenta. The geometric mean of the probabilities by all the 34 models for all samples under the same condition was calculated as a score: If the score value of a condition is above 0.5, then the samples under this condition are more similar to normal placenta, if the score is below 0.5, then

the condition is more similar to FGR. Using all the 34 genes, we found that no condition is closer to the normal placenta; and where the PHT cells were treated with 0% oxygen for 48 hours (condition 3), is closest to the FGR placenta.

Log Likelihood Ratio:
Finally, we calculated the mean vectors μ_n and μ_f, and the covariance matrices Σ_n and Σ_f of the expression levels of the 34 genes for the normal and FGR placentas respectively, (both Σ_n and Σ_f are estimated as diagonal matrices so that their inverses exist.) Then we calculated the log likelihood of each PHT sample under each hypoxic/normoxic condition being generated respectively from a multivariate normal distribution $N(\mu_f, \Sigma_f)$ and a multivariate normal distribution $N(\mu_n, \Sigma_n)$. These log likelihoods are plotted in Figure 2, where the dashed line representing the samples that would be equally likely generated from distributions $N(\mu_f, \Sigma_f)$ and $N(\mu_n, \Sigma_n)$. From the plot, we can see that the PHT samples under various hypoxic/normoxic conditions are overall more likely to be generated from the distribution estimated from the FGR placentas than the distribution estimated from the normal placentas.

<u>Unsupervised Analysis</u>:
In addition to the supervised analysis, we also performed the unsupervised analysis of the gene expression data to explore the relations among the gene expression profiles of the PHT samples under various hypoxic/normoxic conditions and the normal and FGR placentas.

Clustering:
First, we clustered the gene expression profiles of the PHT samples and placenta samples using hierarchical clustering method. We first clustered the expression of all the 34 genes, using the Ward method with Euclidean distance. The dendrogram is shown in Figure 3. It is clear that, from the plot, the in vivo data, consisting of the gene expressions of the 4 normal and 4 FGR placentas, are clustered together tightly and separately from the other PHT samples. Using liner mixed effect models, we found that, even with FDR controlled at 5%, out of the 34 genes, 19 of them are significantly differentially expressed between the placenta sample (including both normal and FGR) and the PHT samples (under various hypoxic/normoxic conditions.) Among the other 15 genes, 2 of them have at least a 2 fold change in average expression levels between the placentas and the PHT samples. We clustered the PHT samples and the placentas again using the expression level of the 13 genes that are not significantly differentially expressed between placentas and PHT samples, and with a fold change of less than 2 between placentas and PHT samples. The resulting cluster is shown in Figure 4. From the dendrogram, we can see that conditions 1 and 7, where the PHT samples are under normoxic condition with 20% oxygen, are the closer to the FGR placentas than all the PHT samples and the normal placentas, where conditions 3, 5, and 6, where the PHT samples were under 0% oxygen for more than 36 hours, form a large cluster separately from all the other samples.

Multidimensional Scaling:
To better visualize the relation among the PHT samples under various hypoxic/normoxic conditions and the normal and FGR placentas, we also employed the classical multidimensional scaling method (MDS) to the gene expression data. Using the classical MDS method, we embedded the 34 dimensional gene expression profile of each sample into a two-dimensional space while preserving the Euclidean distance between the gene expression profiles. From the

plot of the two-dimensional embedding, we can see that the normal and FGR placentas are close to each other but far away from the other PHT samples. Among the PHT samples, condition 1 is the closest to the placenta samples, conditions 8 to 12 are mixed together and close to each other, conditions 5 and 6 are close to each other, and far away from other samples, especially the placentas.

Discussion:

Based on the supervised and unsupervised analyses of the gene expression data of the PHT samples and the placenta samples, we have the following discoveries:

1. The difference in gene expression profiles between the placentas and the PHT samples is much larger than the difference between normal and FGR placenta, and the difference between PHT samples treated under any hypoxic/normoxic conditions.
2. While the expression profiles of the PHT samples are different from those of the placentas, overall they are more similar to the FGR placentas than the normal placentas.
3. The PHT samples under the early injury conditions 8, 9 ..., 12 have very similar expression patterns, suggesting that if treated for only 12 hours, the difference in hypoxic conditions does not cause significant changes in gene expression profile.
4. The PHT samples under the late injury conditions 1, 2 ..., 6 have very different expression profiles, suggesting that if treated for 48 hours, the difference in hypoxic conditions may cause significant changes in gene expression profile.
5. The PHT samples under condition 1 (20% oxygen, 48h) is more similar to the normal and FGR placenta than the PHT samples under condition 2 (8% oxygen, 48h), suggesting that when conduction in vitro experiments, primary trophoblast cells cultured at 20% oxygen may better mimic the in vivo condition than trophoblast cells cultured at 8% oxygen.

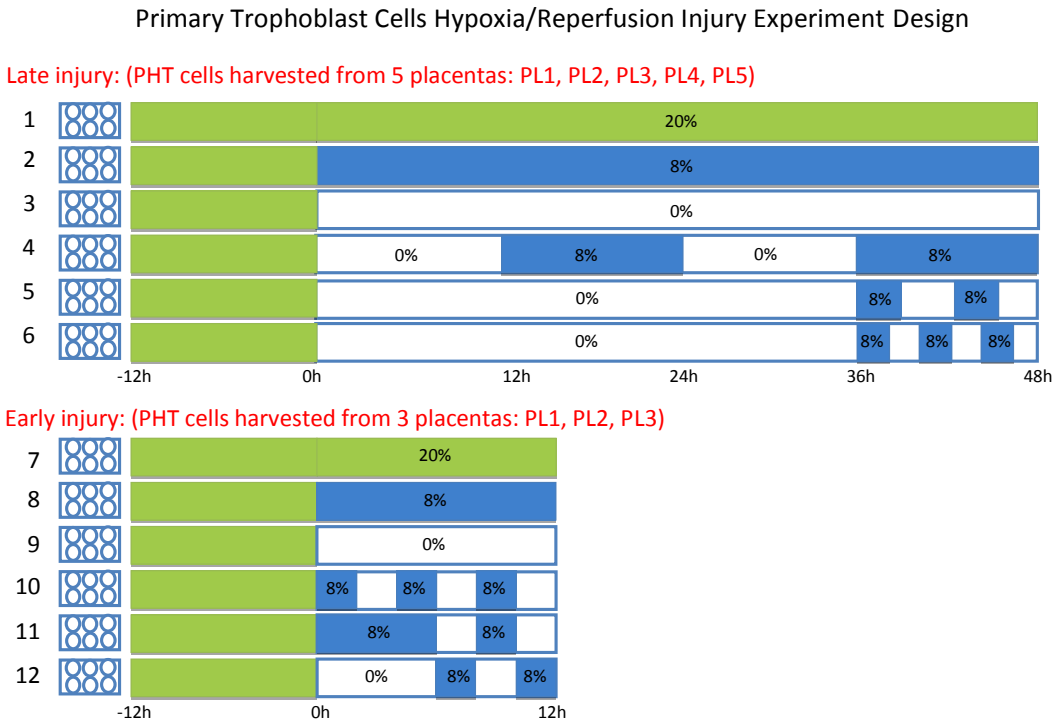

Figure 1. Design of the PHT Hypoxia/Reperfusion Injury Experiment

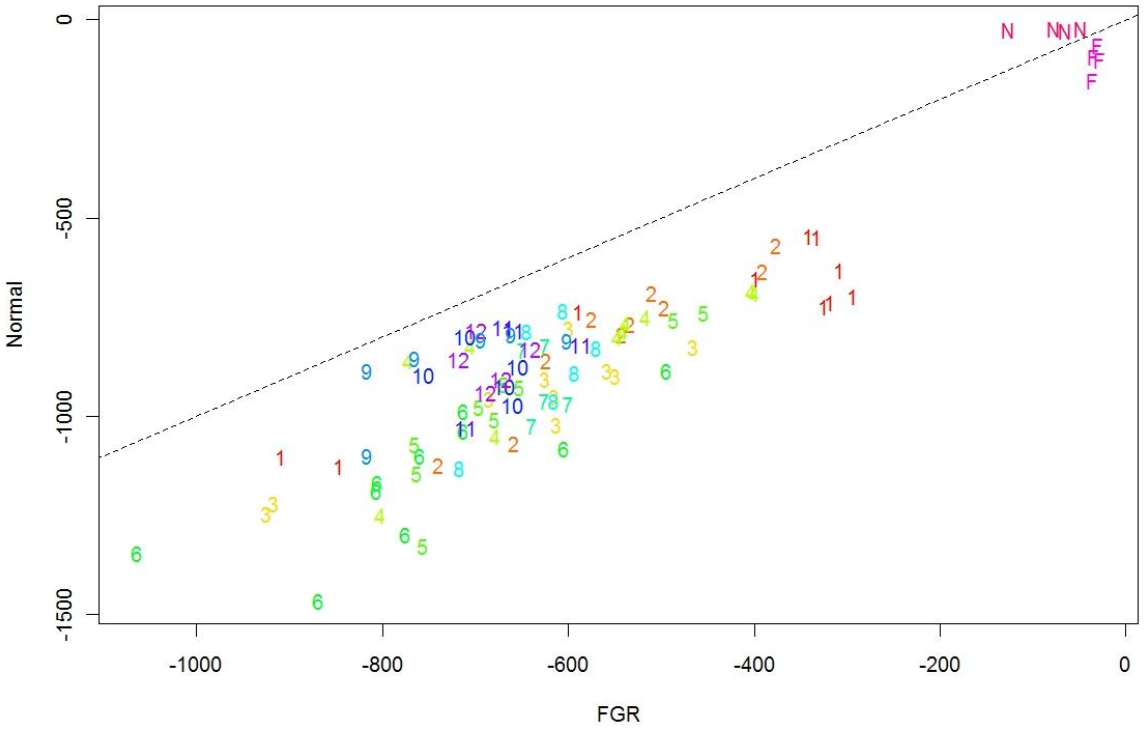

Figure 2. Log Likelihood Ratio of PHT Samples to Placenta Samples

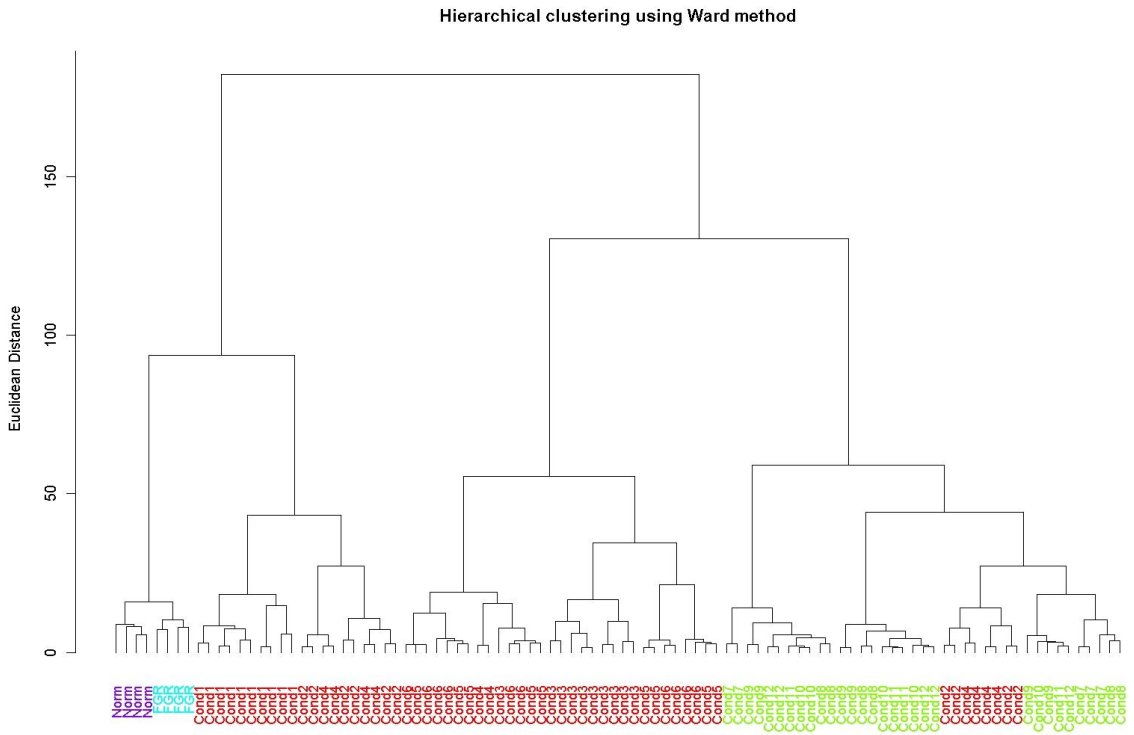

Figure 3. Hierarchical Clustering using all 34 genes

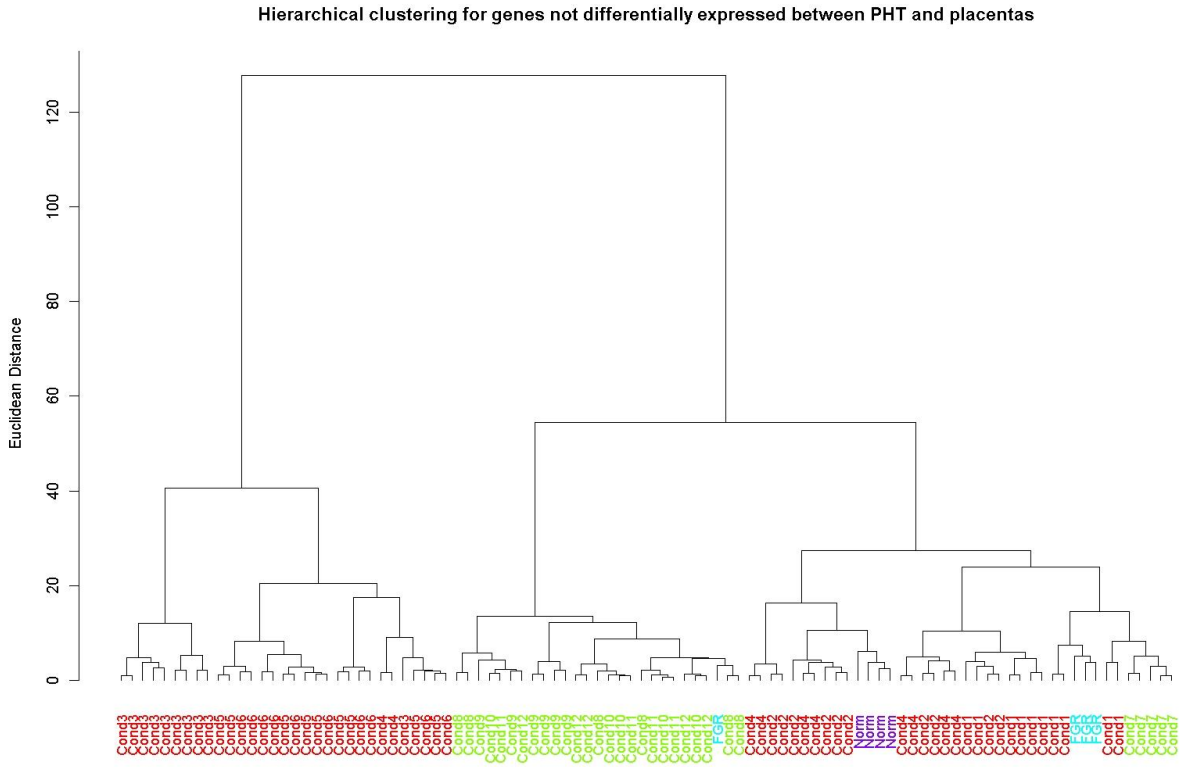

Figure 4. Clustering using 13 genes not differentially expressed between PHT and placentas

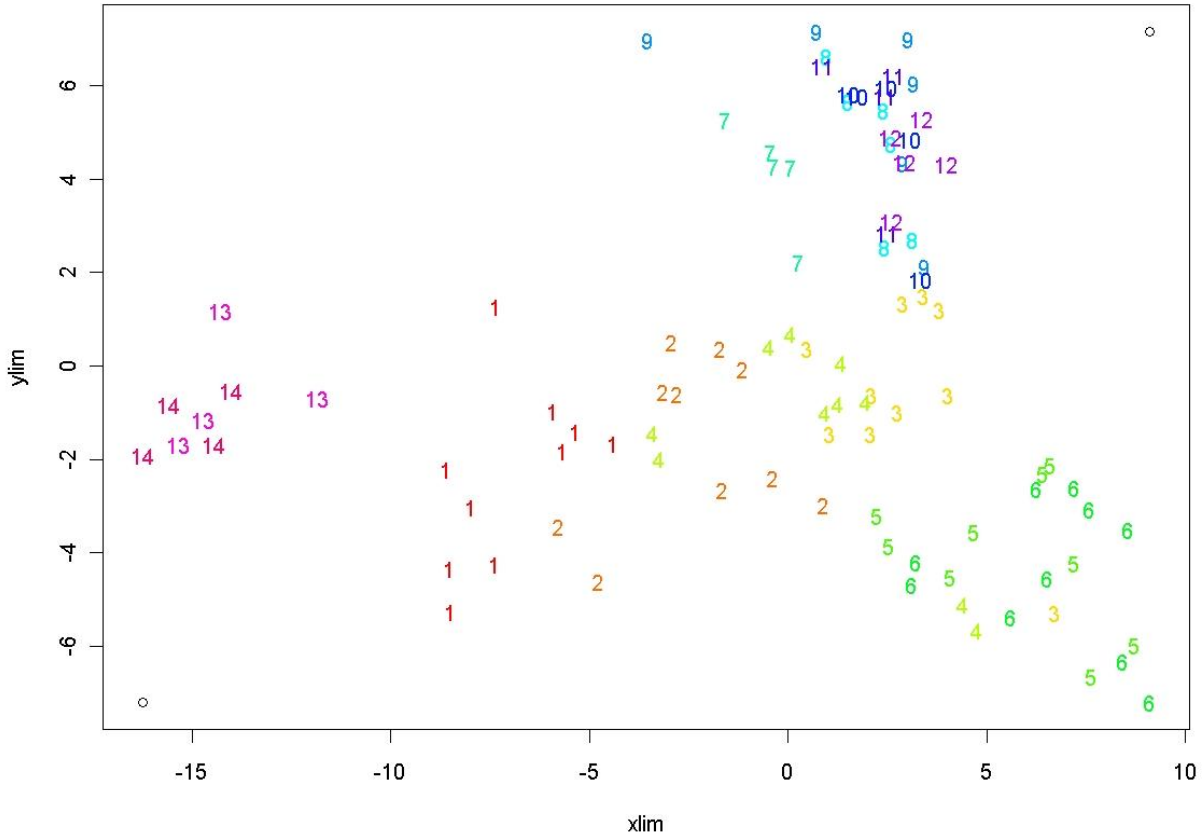

Figure 5. Multidimensional scaling of the gene expression profiles of PHT and placenta samples

<u>Research Project 3: Project Title and Purpose</u>

Hypoxia Inducible miR-210 as a Potential Therapeutic Target in Renal Cell Carcinoma - We plan to illustrate the mechanism of apoptosis in clear cell renal cell carcinoma cells (ccRCC) harboring *VHL* mutation caused by inhibition of a hypoxia inducible microRNA (miRNA), miR-210. By identifying the genes responsible for this phenotype, we will discover potential novel therapeutic targets for ccRCC, which is refractory to current chemo- and radiation- therapies.

Anticipated Duration of Project

1/1/2010 – 12/31/2010

Project Overview

The main objective of this project is to systematically investigate the mechanism of a hypoxia inducible miRNA, miR-210, on ccRCC tumor survival and to examine miR-210 or its target genes as novel therapeutic targets for ccRCC. We have planned a series of mechanistic studies using paired ccRCC cell lines, ccRCC cells with *VHL* mutation ($VHL^{-/-}$, with highly elevated miR-210 expression) and same ccRCC cells expressing reconstituted wild type *VHL* ($VHL^{+/+}$,

with basal low level miR-210 expression). Specifically, we will examine cell survival, proliferation, apoptosis, and metabolism after inhibiting miR-210 expression in *VHL*$^{-/-}$ cells. In addition, we will identify miR-210 targets in these cells by Argonaute 2 immunoprecipitation followed by microarray experiments and will manipulate these identified genes by either shRNA knock-down or ectopic expression to recapitulate the phenotype of miR-210 knock-down, increased apoptosis. Finally, we will investigate the effect of inhibition of miR-210 expression on the sensitivity of ccRCC cells to chemotherapeutic agents. In summary, this project is intended to provide mechanistic insights on miR-210's function in ccRCC survival and to identify novel therapeutic targets for ccRCC.

Principal Investigator

Xin Huang, PhD
Research Assistant Professor
Magee-Womens Research Institute and Foundation
204 Craft Ave., B407
Pittsburgh, PA 15213

Other Participating Researchers

None

Expected Research Outcomes and Benefits

ccRCC is among the tumors most resistant to radiation- and chemo-therapies. Currently, there is no effective treatment for this devastating disease. Our project will address the function of miR-210 in ccRCC apoptosis and survival and illustrate the mechanism of cell death caused by miR-210 inhibition. We expect to identify a list of miR-210 target genes, of which ccRCC cells must repress when the tumor suppressor gene, *VHL* is mutated. These miR-210 target genes or miR-210 *per se* will be attractive targets for developing novel therapy against ccRCC and eventually leading to a better overall survival of ccRCC patients.

Summary of Research Completed

We used RCC4, a clear cell renal cell carcinoma (ccRCC) cell line that harbors a loss-of-function mutation of the *VHL* gene, as the model system to investigate miR-210 function in ccRCC. Here, we summarize our findings to date:

<u>miR-210 is highly expressed in ccRCC cells</u>

ccRCC patients have high frequency of the *VHL* gene mutation (~57-80%). *VHL* is an E3 ubiquitin ligase functioning as a tumor suppressor gene in renal cells by degrading HIFα. We selected two ccRCC cell lines with the identical genetic background, RCC4 and RCC4/VHL to study miR-210 expression. RCC4/VHL cell line was derived from the RCC4 cell line by re-introducing wild-type *VHL* gene into the RCC4 cells. Thus, RCC4 and RCC4/VHL cells are genetically identical other than the status of the *VHL* gene. We confirmed by Western blotting

that HIF1α is stabilized in RCC4 cells as a result of mutated *VHL* gene and reconstituted wild-type VHL gene in RCC4/VHL could efficiently degrade the HIF1α protein (Figure 1, upper panel). We then performed microRNA Northern blotting to detect miR-210 expression in RCC4 and RCC4/VHL cells. Our results clearly demonstrated that miR-210 is highly expressed in RCC4 cells compared to RCC4/VHL cells, reflecting that stabilized HIF1α could up-regulate miR-210 in ccRCC (Figure 1, lower panel). We are currently examining more ccRCC cell lines for miR-210 expression.

Down-regulating miR-210 expression reduces RCC4 cell proliferation

Since miR-210 is highly up-regulated in RCC4 cells with mutated *VHL* gene, in order to investigate miR-210 function we utilized the locked nucleic acid (LNA) technology to knock down miR-210 expression in RCC4 and RCC4/VHL cells. As shown by TaqMan real-time PCR assay in Figure 2A, we efficiently down-regulated miR-210 expression by antisense LNA against miR-210 in both cell lines. Interestingly, when miR-210 is knocked down, cellular proliferation was significantly reduced in RCC4 cells compared to that of in RCC4/VHL cells (Figure 2B). We further investigated the mechanism of reduced cell proliferation after knocking down miR-210 expression. Because apoptosis is a critical factor in regulating cell proliferation, we stained the RCC4 and RCC4/VHL cells with FITC conjugated Annexin V antibody and propidium iodide (PI) after miR-210 knock down and performed flow cytometry analysis. Surprisingly, we only observed slightly increased RCC4 cell apoptosis after miR-210 knock down compared to RCC/VHL (Figure 2C), suggesting that apoptosis alone cannot explain the significantly reduced cell proliferation after miR-210 knock down in RCC4 cells. To dissect the mechanism further, we performed clonogenic cell survival assay to examine cell survival after miR-210 knock down. RCC4 cells were re-plated into 4 plates with 300 or 3000 cells for each plate 24 hours post transfecting LNA against miR-210 or a scramble LNA into RCC4 cells. The cells were then kept growing for two weeks and then, the cells were stained by crystal violet and the colonies were counted. Interestingly, the number of colonies formed in cells transfected with LNA against miR-210 was significantly less than that of in cells transfected with the scramble LNA. The difference in colony formation nicely explained the difference we observed in the cell proliferation assay. Because the reduced colony formation may be contributed to apoptosis, cell cycle arrest (including senescence), and autophagy, we are currently performing experiments to determine the mechanisms responsible for the phenotype.

Down-regulating miR-210 expression sensitizes RCC4 cells to chemotherapeutic drugs

Since ccRCC is among the tumors most resistant to radiation and chemotherapy, we tested whether inhibition of miR-210 could sensitize RCC4 cells to cell death induced by common chemotherapeutic agents, such as Doxorubicin and Camptothecin. We added Doxorubicin and Camptothecin to RCC4 cells 24 hours post miR-210 antisense LNA or a scramble LNA transfection. Interestingly, inhibition of miR-210 significantly sensitized RCC4 cells to Doxorubicin and Camptothecin induced cell death (Figure 3), indicating that mir-210 is a novel therapeutic target for ccRCC.

Identifying miR-210 target genes

To better understand the mechanism of miR-210 in sensitizing RCC4 cells to chemotherapeutic drugs, identification of miR-210 targets is essential. We utilized argonaute protein immunoprecipitation (RNP-IP) followed by the SOLiD next generation sequencing (NGS) to comprehensively identify miR-210 target genes. NGS has a unique advantage in identifying miRNA targets since NGS does not require prior knowledge of the target genes to be sequenced and thus, could potentially identify novel miR-210 targets that otherwise may be missed by conventional microarray experiments. We first established RCC4 and RCC4/VHL cell lines stably expressing a HA-tagged AGO2 protein (Figure 4), which is the major functional component of the RNA induced silencing complex (RISC) where miRNAs' inhibitory function on their target genes is carried out. We then performed RNP-IP assay using an anti-HA antibody to pull-down the AGO2 protein and associated mRNAs. By comparing the immunoprecipitated mRNA profiles between RCC4 and RCC4/VHL cells, we will be able to comprehensively identify miR-210 targets. The immunoprecipitated mRNA samples are currently being sequenced at the University of Pittsburgh Genomics and Proteomics Core Facility (GPCL).

Figures

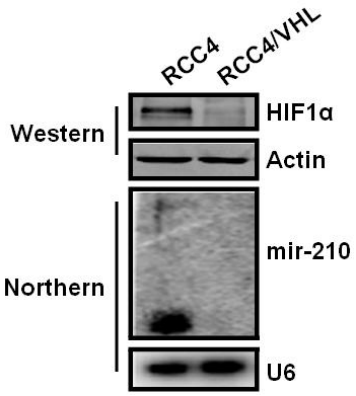

Figure 1. miR-210 is highly expressed in RCC4 cells

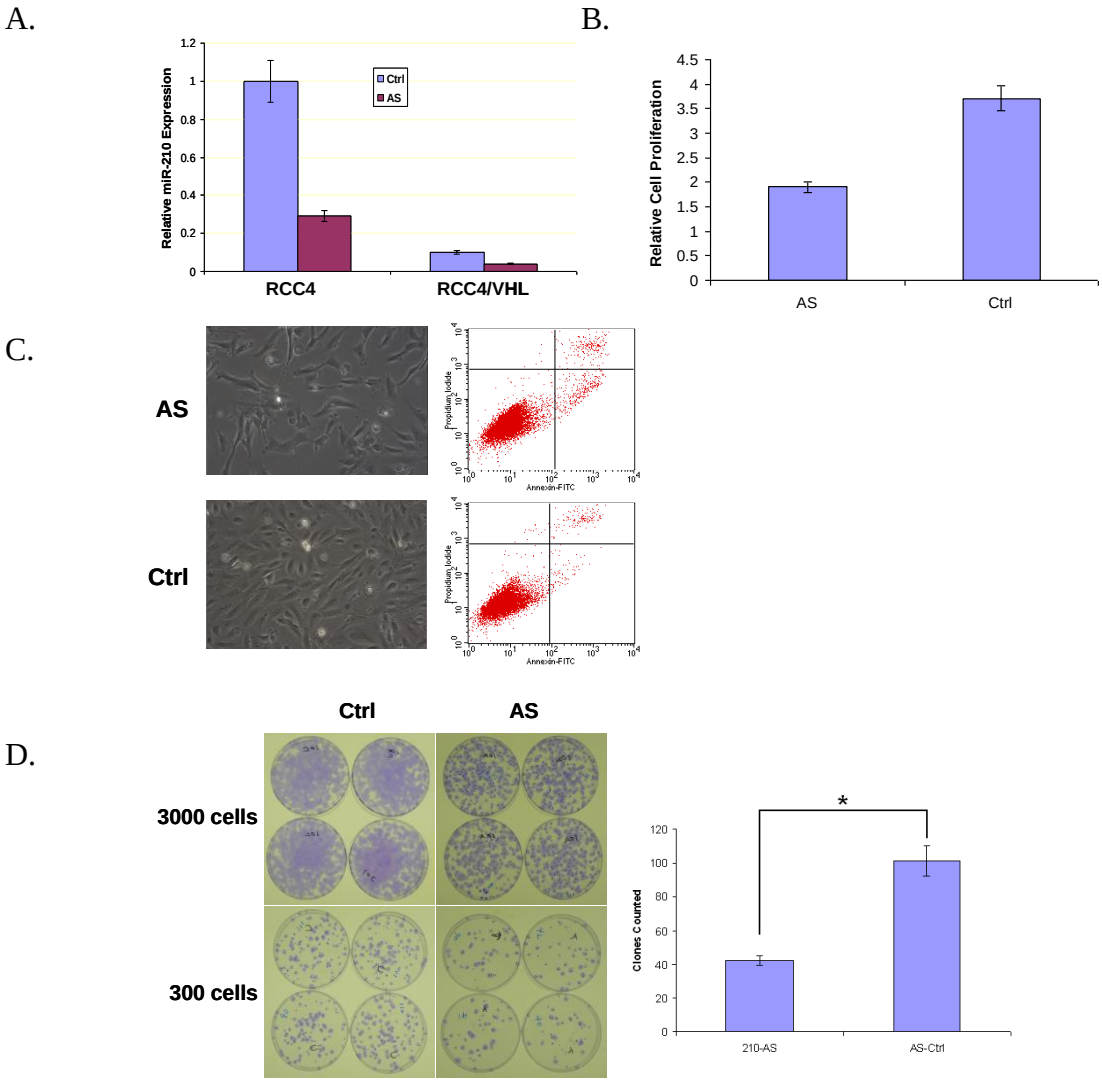

*Figure 2. Inhibition of miR-210 results in decreased RCC4 cell proliferation by reducing cell survival. A. LNA antisense oligo (AS) efficiently knocked down miR-210 expression in RCC4 and RCC4/VHL cells compared to control scramble oligo (Ctrl) measured by RT-QPCR; B. Knockdown of miR-210 results in approximately 2-fold decrease of cell proliferation. Cells are counted 48 hours after transfection; C. Slightly increase of apoptosis is observed by Annexin V staining followed by flow cytometry analysis. D. RCC4 cell survival is significantly reduced after miR-210 knockdown as measured by clonogenic cell survival assay. Right panel, colony quantification for the 300-cell assay. * indicates $p < 0.05$ by two-tailed student's t-test.*

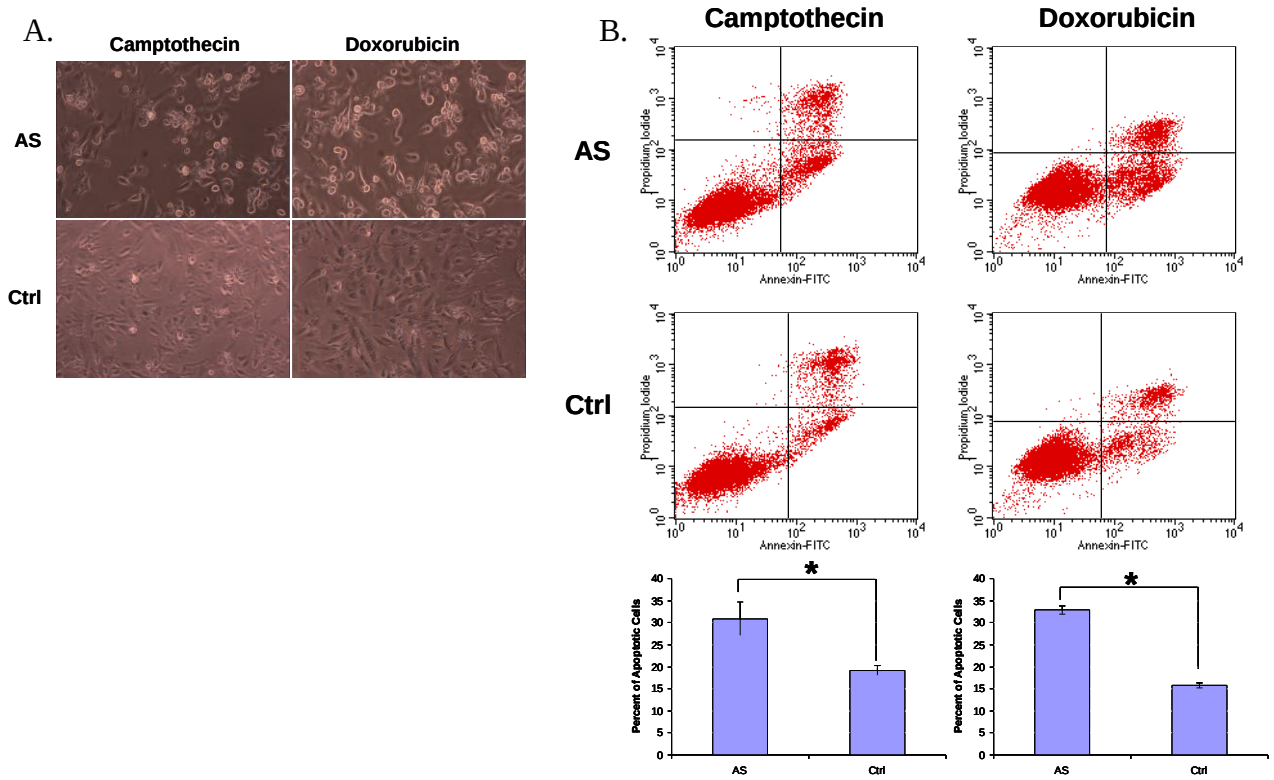

*Figure 3. Inhibition of miR-210 sensitizes RCC4 cells to Camptothecin and Doxirubicin, two common chemotherapeutic drugs. A. Massive cell death is seen in RCC4 cells treated with two drugs while miR-210 is inhibited, but no apparent cell death in cells only treated with the drugs; B. Quantification of apoptosis by Annexin V staining followed by flow cytometry. There is an approximately two-fold increase of apoptosis when inhibition of miR-210 is combined with Camptothecin and Doxirubicin treatment compared to drug treatment alone. * indicates $p < 0.05$ by two-tailed student's t-test.*

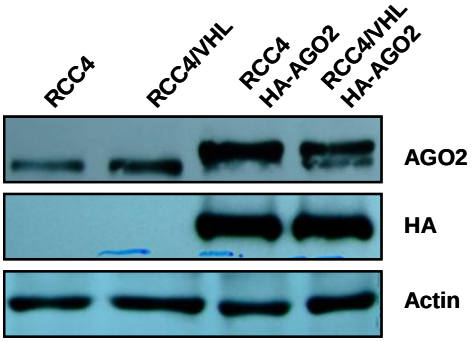

Figure 4. RCC4 and RCC4/VHL cell lines stably expressing HA-tagged AGO2 protein.

Research Project 4: Project Title and Purpose

Role of miR-424 in the Differentiation and Function of Placental Trophoblasts - Our ultimate goal is to understand how hypoxic stress impacts placental function. Feto-placental hypoxia is associated with pregnancy complications but the molecular mechanisms remain poorly understood. We recently found that hypoxia induces major changes in the expression levels of several microRNAs (miRNAs), a family of small regulatory RNAs that are increasingly found linked to disease. One of them, mir-424, is normally abundant in placental trophoblasts but is significantly decreased when cells are exposed to hypoxia. The downregulation of miR-424 could lead to the de-repression of a number of target genes and have profound consequences on the trophoblast biology. This research will focus on the expression and the role of miR-424 in the differentiation of placental trophoblasts.

Anticipated Duration of Project

1/1/2010 - 12/31/2010

Project Overview

Placental insufficiency is one of the main complications of pregnancy and is associated with compromised fetal development and poor outcome. Failure of the placenta to fulfill its function is often associated with feto-maternal hypoxia. Whereas incompletely understood, recent studies have shown that hypoxic stress significantly alters gene expression in placental trophoblasts and impairs their differentiation. In order to interrogate the molecular changes brought about by hypoxic stress, we recently performed several miRNA profiling experiments in human primary trophoblasts that were cultured in either standard oxygen conditions (FiO_2=20%) or in hypoxic conditions (FiO_2=1%). Among a set of differentially regulated miRNAs we found that miR-424, a normally abundant miRNA, is significantly reduced in hypoxic trophoblasts. As miRNAs have the potential to regulate many target genes, this could affect differentiation pathways of trophoblasts. Consistent with this hypothesis, we identified two targets of miR-424 that were downregulated in placental trophoblasts exposed to hypoxia. In the genome, miR-424 is found in an intergenic region located on the chromosome X and in a cluster with five other miRNA genes that may be co-regulated. This feature may even further expand the regulatory potential of the miRNAs from this genomic region. Interestingly, this cluster is conserved across mammals including the mouse and we detected several miRNAs from this region in mouse placentas. It is our hypothesis that hypoxia affects the expression of several members of this miRNA cluster leading to the de-repression of several genes involved in the control of trophoblast differentiation. To test this hypothesis we will first analyze the impact of miR-424 on the cellular functions of primary trophoblasts. To this end we will inhibit the function of miR-424 and some of its targets in trophoblasts and analyze the cellular consequences. Finally, we will further characterize the expression profile of this cluster in the human placenta as well as the mouse placenta.

Principal Investigator

Jean-Francois Mouillet, PhD
Research Instructor
University of Pittsburgh
Department of OBGYN and Reproductive Sciences
Magee-Womens Research Institute
204 Craft Avenue, Room A634
Pittsburgh, PA 15213

Other Participating Researchers

Yoel Sadovsky, MD, Magdalena Jennings - employed by University of Pittsburgh

Expected Research Outcomes and Benefits

Our long-term goal is to understand the response of the human placenta to injury, and in particular to low oxygen (hypoxic) stress. This knowledge will pave the way for the design of new preventive measures to decrease the impact of placental injury on the developing fetus. Low placental oxygenation is one of the main stress conditions in the human placenta and is believed to play a role in the development of pathologies such as intrauterine growth restriction (IUGR) and hypertension of pregnancy. These conditions are associated with increased perinatal illnesses and mortality. Newborns surviving these insults are at risk for lifelong complications, including developmental diseases and a greater incidence of the adult metabolic syndrome (type-2 diabetes, high lipids, hypertension, obesity and related illnesses). Despite the well-documented association between hypoxia and these conditions, little is known about the mechanisms involved in the development of these defects.

Oxygen plays a major role in the differentiation of placental cells that occurs during pregnancy. We recently performed several experiments of placental cells cultured in low oxygen conditions to mimic placental hypoxia and examined changes in gene expression. This screen led to the identification of several genes including small RNA molecules (called microRNAs) whose expression is altered in hypoxia. In this project we focus on a novel pathway of gene regulation in the human placenta centering on regulation in the context of hypoxia. Results from our experiments on miR-424 are likely to advance our knowledge on previously unknown pathways that are activated during hypoxia and their role in placental response to injury.

Summary of Research Completed

The human placenta expresses a multitude of miRNAs, particularly in the trophoblast layer. We recently showed that trophoblast cells that have been exposed to hypoxia express reduced levels of miR-424. Because miR-424 is normally highly expressed in the placenta and is predicted to silence numerous targets, this reduction could have a profound impact on trophoblast cells. Interestingly, miR-424 is located within a 7 kb region of the X-chromosome that contains five other miRNA genes, raising the possibility that these miRNAs belong to a cluster.

During the six first months of funding for this project, we initiated a series of experiments aiming at better understanding the role of miR-424 in placental trophoblasts. We have made the following progress on the specific aims described in the original proposal.

Aim 1: Analyze the impact of miR-424 on the cellular functions of primary trophoblasts.

Preliminary experiments led us to the identification of two potential targets for miR-424, FGFR1 and MAP2K1. We first conducted experiments to analyze the targeting of these genes by miR-424. Using a computational search for potential miR-424 binding sites, we identified three seed matches, located at positions 885-891, 888-894, and 1975-1981 within the FGFR1 3'UTR, and only one site in the 3'UTR of MAP2K1 (position 463-469). The 3'UTR sequences of both genes were PCR amplified from genomic DNA and cloned into the luciferase reporter vector psiCHECK-2 (Promega). Then using PCR-based mutagenesis, we introduced inactivating mutations in each of the target sites defined by TargetScan and for each of the two targets. We also generated an expression vector for miR-424 by cloning a 437 bp fragment of genomic DNA centered on the sequence of the miR-424 hairpin into the pcDNA3 plasmid (Invitrogen).

In the case of FGFR1, the two first sites are actually overlapping and were counted as one site. Finally, four constructs were tested for FGFR: psiCHECK2-FGFR1-WT, psiCHECK2-FGFR1-mut1, psiCHECK2-FGFR1-mut2, and psiCHECK2-FGFR1-mut1+2. Each construct was transfected in the trophoblast cell line HTR8 and assayed for luciferase activity. Although HTR8 cells express miR-424, influence of the mutations was minimal. However, it is known that upon transient transfection, cells tend to accumulate large amounts of plasmid reporter that may overwhelm the endogenous silencing capacity of these cells. Therefore, we repeated these experiments, including a plasmid expressing miR-424 under the control of a CMV promoter in order to boost the miR-424-mediated silencing potential of these cells. In the presence of the added miR-424, we observed a 60% reduction of the activity of the reporter containing the wild-type (WT) form of FGFR1-3'UTR. Interestingly, removing the nucleotides corresponding to the seed match of the first target site (mut1) led to a complete loss of silencing by miR-424. Of note, this site is broadly conserved across vertebrate species. In contrast, mutations in the second (mut2), less conserved site, had no influence on the activity of the reporter. Altogether, these experiments confirm the functionality of the conserved miR-424 target site in FGFR1-3'UTR.

A single miR-424 target site was identified in the 3'UTR of MAP2K1 and mutated. Unexpectedly, when our psiCHECK2-MAP2K1-WT and psiCHECK2-MAP2K1-mut constructs were tested in HTR8 cells, both were equally silenced in the presence of transfected miR-424. However, a closer examination of the sequence of our construct revealed *punctual* nucleotide *sequence divergences* when compared to the published sequence of MAP2K1 (NM_002755). Finally, a BLAST search revealed that the construct actually contains the sequence of a pseudogene referred to as MAP2K1P1. This pseudogene is likely to derive from a mature MAP2K1 mRNA that underwent retrotransposition and became integrated in chromosome 8. Interestingly, sequence examination of the pseudogene showed the presence of a single nucleotide mutation in the seed-match region of the mir-424 target site. We also observed another divergence downstream, which actually resulted in a new miR-424 seed match indicating a potential target site that may explain why mutation of the identified site did not abolish silencing by miR-424. Upon re-sequencing several of the original clones, we identified plasmids

containing the true sequences of MAP2K1. Surprisingly, in our luciferase-reporter assay, the 3'UTR of MAP2K1 did not mediate silencing by miR-424 despite the presence of a predicted conserved binding site. Therefore, it appears that only the pseudogene contains a functional miR-424 target site. Although most retrotransposed genes are not expressed, some are inserted in the vicinity of promoters that can direct their expression. In order to check for this possibility, we performed RT-PCR experiments using a set of primers specific to MAP2K1 and MAP2K1P1. Using this approach, we detected the expression of MAP2K1 in primary trophoblasts but failed to detect any expression of the pseudogene.

Aim 2: Examine the expression of miR-424 and associated species in the human and mouse placenta.

Preliminary Northern blot experiments revealed high expression of miR-424 in primary human trophoblasts with a reduced expression when cells are exposed to hypoxia. Since miR-424 is located in a genomic region that contains several other miRNA genes in close proximity (~6.5 kb) we investigated the possibility that they are co-expressed.

We first examined the relative expression of the miRNA species from this cluster using real-time qPCR. Primary trophoblasts isolated from four different placentas were cultured over a period of 48 h in standard conditions (FiO_2=20%) or in reduced oxygen (FiO_2=1%). Total RNA was extracted with the TRI-Reagent method and treated with DNase I using the TURBO DNA-free from Ambion according to the manufacturer's protocol. Individual miRNA species from the cluster were then quantified using the miScript PCR System from Qiagen. Some miRNA precursors potentially give rise to two mature miRNAs (miR-424, miR-542, and miR-450b), while the two separate genes miR-450a-1 and miR-450a-2 produce the same mature miRNA yielding a total of eight potential mature miRNAs from this cluster (Fig.1). It is usually thought that only one of the two strands from the stem-loop is biologically active while the other one (the passenger strand or miRNA*) is degraded. However, the situation is not clear for all the species. Therefore, a total of eight distinct mature miRNAs are potentially produced by this genomic region.

Results from real-time PCR experiments confirmed the lesser accumulation of miR-424 in human primary trophoblasts exposed to hypoxic conditions. Interestingly, we observed the same trend for all the other miRNAs from the cluster although most of them were expressed at low levels in human primary trophoblasts. For example, the second most expressed miRNA (miR-503) was detected at the same level as miR-424*, the passenger strand of miR-424. The miRNA species located further downstream such as miR-542 and miR-450 were expressed at even lower levels.

We then investigated the expression of the ortholog miRNA cluster in the mouse placenta. The structure of the cluster is well conserved in the mouse and encodes several miRNAs that are perfectly identical to their human counterparts while most of them differ by only one nucleotide. The mouse cluster however, contains an additional mouse-specific miRNA gene (miR-351) intercalated between miR-503 and miR-542 (Fig. 2). We first performed Northern blot analysis of miR-322 (orthologous to human miR-424) and compared its expression in various mouse tissues including placenta, brain, heart, liver, spleen, kidney, skeletal muscle, ovary, and

intestine. Total RNA (20 μg) was resolved on a 15% acrylamide/urea gel, electrotransfered onto a nylon membrane (Hybond N+, Amersham/GE), and hybridized at 37ºC using an oligo-DNA probe labeled with 32P using the StarFire system (IDT). As expected, we observed high expression of miR-322 in the mouse placenta. High expression of miR-322 was also detected in the ovary, while it was detected at moderate or low levels in the other tissues.

Using this Northern blot assay, we also investigated the expression of several members of the miR-322/424 cluster including miR-351 and miR-450a. Interestingly, all of these miRNA species exhibited the exact same pattern of expression across the various tissues assayed. This result suggests again that these miRNAs are co-regulated and truly belong to a genomic cluster. In contrast to human miRNAs, however, it seems that most species from this cluster are expressed at a relatively high level in mice. Although only miR-322 produced a very strong signal in northern blot, we had no problem detecting the two other species, which showed a fairly robust signal. The sequence of the three miRNA species investigated are sufficiently different to exclude non-specific hybridization.

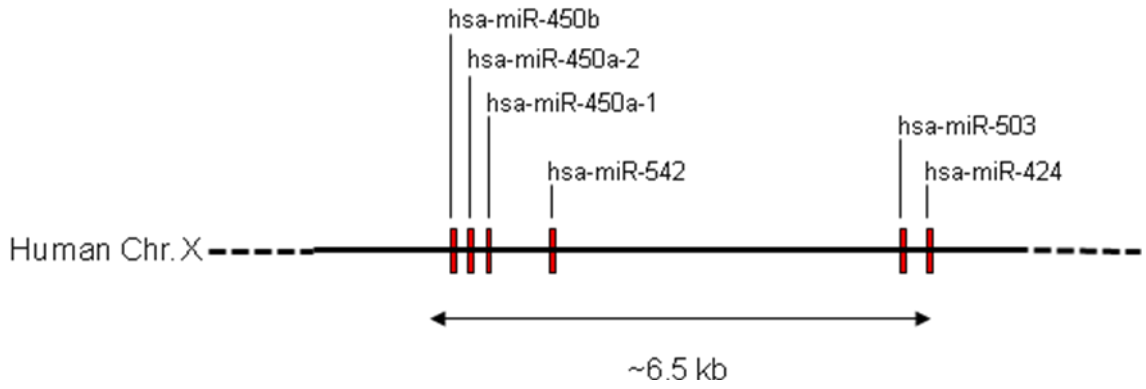

miR-424 stem loop hsa-miR-424 hsa-miR-424*	```---------- a c aa g u cgagggg ua agcagc uucauguuuugaa ugu c ||||||| || |||||| |||||||||||| ||| u gcucccc au ucgucg gagugcaaaacuu gua a gggguggaagauggaaggggu c a cg g a```
miR-503 stem loop hsa-miR-503	```a u g gu a ugcccu gcagcgggaacagu cu ca gagcg u |||||| |||||||||||| || || ||||| c auggga cgucgccuuuguua gg gu cucgu g c u g -- g```

miR-542 stem loop
hsa-miR-542-5p
hsa-miR-542-3p
	``----------caga auc gg uca -a c
	ucucagac ucgg auca ugucacgag uac a
	|||||||| |||| |||| |||||||| |||
	agggucug aguc uagu acaguguuc gug g
	acuucuacucaccg gaa aa uag ac u```
	``-ccaaagaaa u uuu u aa
	gaugc aaacuau ugcga guguuccuaauaugu u
	||||| ||||||| ||||| |||||||||||||| a
	cuaug uuugaua acguu uacagggguuaugua u
	gguauaauaa u cuu u aa```
	``--aaac u uuu u cac
	gauac aaacugu ugcga guguuccuaauaug u
	||||| ||||||| ||||| ||||||||||||| a
	cuaug uuugaua acguu uacaaggguuauau u
	auauaa u ugu u aaa```
	``-- uuu u u g ug aa
	gcagaauuau ugcaa aug uccu aaua u u
	|||||||||| ||||| ||| |||| |||| | a
	uguuuugaua acguu uac aggg uuau g u
	ua ccu u u - gu aa```

Fig. 1: Genomic organization of the human miR-424 cluster and sequences of the predicted stem-loop structures. The right column indicates the name of the predicted stem loop structure (grey background) and the names of the mature miRNAs. The left column depicts the hairpin base-paired structures as predicted in miRBase with the mature miRNAs marked in red. From Griffiths-Jones S, Grocock RJ, van Dongen S, Bateman A, Enright AJ. NAR 2006 34(Database Issue):D140-D144.

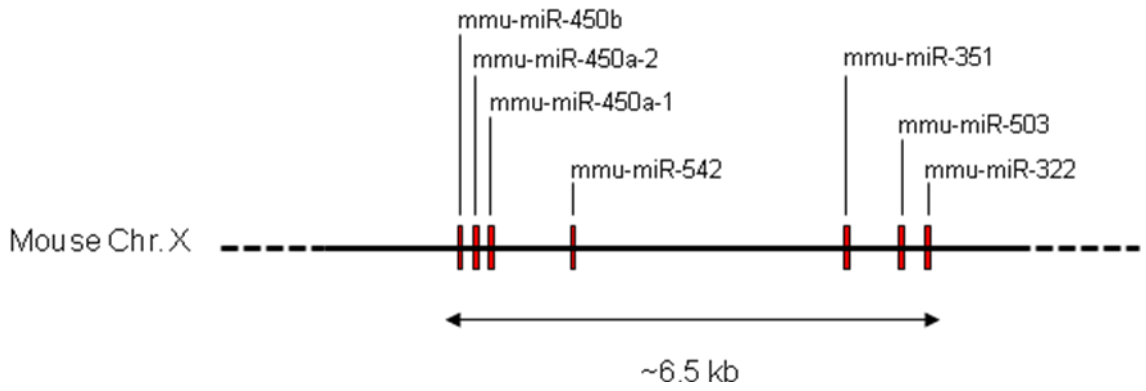

miR-322 stem loop mmu-miR-322 mmu-miR-322*	ccucguuga - c ca aa g auu cuc cgaaggg ug gcagc uucauguuuugga u g ||| ||||||| || ||||| ||||||||||||| | ggg gcuuccc ac cgucg aaguacaaaacuu g c ------aag u c aa cg g aac
miR-503 stem loop mmu-miR-503 mmu-miR-503*	ua c g u a gu ugccc gcag gggaacaguacu cag g gu u ||||| |||| ||||||||||| ||| | || u auggg cguc ccuuuguuauga guc c cg g uc a g - - ug
miR-351 stem loop mmu-miR-351	----ca ---- u ug a c g gagugaa uggcac cuccg uuccc agg gcc uuuga ccug a |||||| ||||| |||||| ||| ||| ||||| |||| auugug gaggu aaggg ucc cgg gaacu ggac a cuucaa agaa c -- g a - aaaaaaa
miR-542 stem loop mmu-miR-542-5p mmu-miR-542-3p	a g c gg uca -a c gg ucucagac u ucgg auca ugucacgag uac a || |||||||| | |||| ||||| |||||||| ||| cc agggucug a aguc uagu acaguguuc gug c g g a aa uag cc u
miR-450a-2 stem loop mmu-miR-450a-5p mmu-miR-450-3p	uuu u uac gaacuau ugcga guguuccuaauaug u ||||||| ||||| ||||||||||||| a cuuggua acguu cguagggguuauau u cuu u gag
miR-450a-1 stem loop mmu-miR-450a	--gaga u u u ugc gauac gagcuguuu ugcga guguuccuaauaug u ||||| |||||||| ||||| ||||||||||||| a cugug uucgauaaa acguu uacaaggguuauau u acauaa u u u uaa
miR-450b stem loop mmu-miR-450b-5p mmu-miR-450b-3p	uuu u g auaa gauacagaauuau ugcag auguuccu aauac c ||||||||||||| ||||| |||||||| ||||| a cuauguuuuaaua acguu uacaaggg uuaug u cgu u - cgaa

Fig. 2: Genomic organization of the mouse miR-322/miR-424 cluster and sequences of the predicted stem-loop structures. The right column indicates the name of the predicted stem loop structure (grey background) and the names of the mature miRNAs. The left column depicts the hairpin base-paired structures as predicted in miRBase with the mature miRNAs marked in red. From Griffiths-Jones S, Grocock RJ, van Dongen S, Bateman A, Enright AJ. NAR 2006 34(Database Issue):D140-D144.

Research Project 5: Project Title and Purpose

Epigenetic Analysis of Human Aneuploidy - Common chromosomal disorders resulting in live births include Down, Turner, Edwards and Klinefelter Syndromes. Although our knowledge of human aneuploidy has improved, there are still many gaps in our understanding of the mechanisms by which an altered number of chromosomes can lead to a specific disease phenotype. One area that has not been previously explored is the effect of aneuploidy on DNA methylation patterns. This is significant because appropriate DNA methylation is known to play a central role in gene regulation and normal homeostasis. This pilot project will therefore characterize genome-wide DNA methylation patterns in normal pregnancies and compare these to aneuploid pregnancies. A practical outcome of this work will be the identification of potential diagnostic biomarkers of human aneuploidy.

Anticipated Duration of Project

1/1/2010 - 12/31/2010

Project Overview

DNA methylation is emerging as a key component of a broad repertoire of epigenetic mechanisms by which normal genome function and balanced homeostasis are maintained. However, we have only a limited understanding of the global organization of DNA methylation patterns and how they impact on gene regulation. DNA methylation patterns are highly tissue specific and are carefully organized and distributed across the genome in a fashion that is tightly regulated. We are interested in the consequences of an aneuploid state on the patterning of the DNA methylome and the possibility that global organization of DNA methylation is disrupted by the presence of an extra chromosome such as in trisomy 21. In addition to our interest in the biological basis of DNA methylation, we also hypothesize that the identification of DNA methylation patterns that are specific to aneuploidy may drive developments in fetal diagnostics via the discovery of biomarkers for the selective amplification of placental DNA from maternal plasma. Such markers could be exploited for the selective amplification of the fetal genome from maternal plasma DNA and the subsequent non-invasive diagnosis of fetal aneuploidy. Similar approaches have generated great excitement because definitive prenatal diagnosis of aneuploidy is currently performed using chorionic villus sampling (CVS) or amniocentesis. These are invasive, expensive and somewhat risky approaches that must be performed by experienced clinicians and are generally only offered to expectant mothers considered to be at elevated risk of carrying a genetically abnormal fetus. The guiding hypothesis of this project is that DNA methylation patterns in the placental villus of aneuploid pregnancies are markedly different than those of their normal euploid counterparts. Therefore, our primary aim is the comprehensive characterization of the placental DNA methylome in cells derived from chorionic villus samples obtained at the beginning of the first trimester from euploid and aneuploid pregnancies. To achieve this goal we will use a high-throughput microarray-based approach to compare methylation at approximately 27,000 CpG dinucleotides in genomic DNA isolated from CVS tissue and (cells cultured from these tissues) of approximately 24 aneuploid pregnancies and 24 normal controls. This approach will identify regions of DNA that are differentially methylated

between these tissues on a genome wide scale. This information will serve as a foundation for both the future development of non-invasive tests for fetal diagnosis and the development of our understanding of how aneuploidy affects the structure of the DNA methylome.

Principal Investigator

David G. Peters, PhD
Associate Professor
University of Pittsburgh
Magee-Womens Research Institute
204 Craft Avenue
Pittsburgh, PA 15213

Other Participating Researchers

Patricia Shaw, BS - employed by University of Pittsburgh Medical Center
Tianjiao Chu, PhD - employed by University of Pittsburgh

Expected Research Outcomes and Benefits

Major outcomes of this project will be the identification of regions of the human genome that are methylated in normal CVS tissues and the identification of locations at which these methylation marks are altered in samples from normal and aneuploid pregnancies. This information will provide insight into the biological significance of DNA methylation in these cells in a genome wide fashion and will develop our understanding of the epigenetic consequences of an altered number of chromosomes. Furthermore, these insights will identify regions of the genome where DNA methylation is altered in specific diseases such as Down, Turner, Edwards and Klinefelter Syndromes. There is currently great interest in the development of non-invasive diagnostic tests for fetal genetic disease that rely upon the analysis of cell free DNA obtained from maternal plasma. Such DNA samples contain detectable amounts of DNA derived from the placenta that can be used to genotype the fetus in a non-invasive fashion. One of the challenges in this field is distinguishing maternally inherited fetal alleles from identical endogenous maternal DNA. One approach to overcoming this barrier is to exploit unique placental DNA methylation patterns. Therefore, the differentially methylated regions we identify may provide us with methylation based diagnostic markers for the early detection of fetal aneuploidy using DNA obtained from maternal plasma. Such biomarkers would be defined by their ability to distinguish between normal and aneuploid fetuses. The development of such markers into routine clinical tests could enable the accurate diagnosis of fetal genetic disease during early gestation using DNA derived from maternal plasma samples. Such an approach would largely remove the requirement for invasive methods of diagnosis such as CVS or amniocentesis. In summary, this research project will greatly improve our understanding of DNA methylation in the context of aneuploidy and could lead to the development of noninvasive tests for the accurate diagnosis of related fetal genetic diseases in expectant mothers.

Summary of Research Completed

Background and Specific Aims

Despite the intense interest in epigenetics and the importance of its function in normal development there is no literature that characterizes the placental DNA methylome in early gestation. *This study therefore presents a unique opportunity to answer critical questions relating to human epigenomics in the context of placental function and aneuploidy*. We hypothesize that placental DNA methylation patterns, specifically within the chorionic villus and in cells derived from this tissue, have distinct characteristics that are altered between normal and aneuploid genomes. We further hypothesize that differences in DNA methylation have the potential to be exploited via the development of non-invasive methods based upon selective amplification of fetal DNA from maternal plasma. We will test these hypotheses by carrying out the following specific aims.

1. We will generate high-resolution quantitative maps of DNA methylation in CVS tissue and cultured cells derived from CVS using the Illumina Humanmethylation27 microarray platform. Samples to be used in these experiments have already been collected from normal and aneuploid pregnancies.

2. We will confirm DNA methylation changes identified using microarray based approaches (Aim 1) at the single gene level using Sequenom-based Epityper assays.

Results to Date

DNA was extracted from a total of twenty-four tissue samples/cultured cell samples according to the scheme in Table 1. Briefly, we have thus far analyzed DNA from a total of six karyotypically normal chorionic villus (CV) samples and five trisomy 21 snap frozen CV tissue samples. We further analyzed DNA from a total of four karyotypically normal and four trisomy 21 cultured CV cell samples. Some of the latter were analyzed in duplicate to generate technical replicate data.

DNA was used to interrogate two 12x HumanMethylation27 oligonucleotide microarrays (Illumina). This platform allows the analysis of 27,578 CpG sites per sample at single-nucleotide resolution. The HumanMethylation27 panel targets CpG sites located within the proximal promoter regions of transcription start sites of 14,475 consensus coding sequencing (CCDS) in the NCBI Database (Genome Build 36). In addition, 254 assays cover 110 miRNA promoters.

The resulting data were analyzed using novel statistical tools (see Materials and Methods). Specifically we carried out the following comparisons. First we identified CpG sites that are differentially methylated between karyotypically normal and trisomy 21 samples regardless of whether the data were obtained using fresh CV tissue or cultured CV-derived cells. Two lists of statistically significant genes were identified to represent those CpGs that are more or less methylated in trisomy 21 samples compared to normal samples. The top ten most statistically significant genes in each case are listed in Tables 2A and 2B respectively.

Significantly, we found that hierarchical clustering of all the samples identified a clear distinction between two groups of samples (Figure 1). Rather than delineating differences

between normal and trisomy 21 samples, this distinction between clusters was representative of whether the samples were derived from fresh frozen CV tissue or cultured CV-derived cells.

We therefore carried out a second group of analyses in which we separated uncultured and cultured samples into two groups and treated them separately. Table 3A and 3B show the top ten CpG sites found to be more or less highly methylated, respectively, between fresh frozen CV tissue from normal and trisomy 21 pregnancies. Table 3C and 3D show the top ten CpG sites found to be more or less highly methylated, respectively, between cultured CV-derived cells from normal and trisomy 21 pregnancies.

Materials and Methods

CV Tissue Handling
All samples used in this study were discarded de-identified tissues. CV samples were obtained between gestational weeks 11 and 13 from the Magee Women's Hospital Cytogenetic Screening Laboratory. Samples were dissected under a microscope and separated from any decidual tissue or flecks of blood. The culture media was removed and the tissue placed in 1.5 -2.0mL microcentrifuge tubes before freezing at -80°C until DNA was extracted.

DNA Extraction from CV Tissue
To extract DNA, one 5mm stainless steel bead and 180μL buffer ATL (from Qiagen's DNeasy Blood and Tissue kit) were added to each CVS sample. The samples were placed in the TissueLyser (Qiagen) Adaptor set 2 x 24, and the TissueLyser was operated for 20 seconds at 30Hz. The DNA was then purified using the DNeasy Blood and Tissue kit (Qiagen) as per the manufacturer's protocol.

DNA Extraction from CV-Derived Cells
DNA then purified using the DNeasy Blood and Tissue kit (Qiagen) as per the manufacturer's protocol.

Infinium Microarray Analysis
The HumanMethylation27 DNA Analysis BeadChip (Illumina) allows interrogation of 27,578 CpG sites based on the NCBI CCDS database (Genome Build 36) and also targets the promoter regions of 110 miRNA genes. Bisulphite conversion of DNA was carried out using the EZ DNA Methylation™ Kit (Zymo Research Corp., CA) to convert unmethylated cytosine nucleotides to uracil. Following denaturation with 0.1N NaOH, converted DNA samples were amplified by incubation at 37ºC for 20 hours in a proprietary amplification reaction mix. Amplified DNA was fragmented using vendor-supplied reagents by incubation for 1 hour at 37ºC. Fragmented DNA sample was precipitated and resuspended in hybridization buffer. Infinium BeadChips were cleaned and activated by washing with ethanol, formamide and vendor supplied pre-hybridization buffers. DNA samples are denatured, applied to the Infinium arrays and hybridized 16-24 hours with rocking at 48ºC. The BeadChip is placed into a flow-through chamber, unhybridized and non-specifically hybridized DNA was washed away and single base extension was performed on bound primers with labeled nucleotides. Hybridized DNA sample was removed by washing using proprietary buffers. Staining steps were performed to attach florescent dyes to the labeled nucleotides and the array surface sealed to protect the dyes from

atmospheric degradation. The final array was scanned using an Illumina BeadArray Reader and the data analyzed using Bead Studio 2.0.

Determination of the methylation status of CpG sites using Infinium Array Data
On an Infinium array, each targeted CpG site is interrogated by 2 probes: probe A for unmethylation status, and probe B for methylation status. The A probe signals and B probe signals are normalized separately, using the cyclic loess algorithm. We then compute the log ratio of probe B to probe A: log(B/A), as well as the beta value, which is defined as approximately B/(A+B+100), assuming A,B≥0. Both beta and log(B/A) can be used as a measurement of the methylation level of a CpG site. In particular, a CpG site is hypomethylated if the log(B/A) value of that site is significantly lower than 0. It is hypermethylated if log(B/A) is significantly higher than 0. Student's t tests are used to test if a CpG site is methylated in a group of samples, or if two groups of samples have identical methylation rate at a given CpG site. Empirical Bayesian method is used to estimate the within group variance. P values are adjusted using Benjamini and Hochberg method to control the false discovery rate (FDR) at 5%. Microarray data were clustered using the agglomerative hierarchical clustering method using the R statistical package. Each sample was treated as a 27,578-dimension vector (there are a total of 27,578 probes in an array). The Euclidean distance between samples was used as the distance metric.

Discussion and Next Steps
We have generated genome wide data that begins to characterize the differences between trisomy 21 and normal in CpG DNA methylation patterns obtained from both fresh frozen CV tissue and cultured CV-derived cells. As shown in Figure 1, there are striking differences between methylation patterns identified in karyotypically normal versus trisomy 21. This indicates that the process of cell culture either causes *de-novo* changes in DNA methylation or results in cell-type selection and subsequent loss of other cell types that are present, and can therefore contribute to the molecular phenotype, in un-cultured samples. Further computational analysis and experimental comparison will therefore not involve the analysis of both uncultured and cultured samples in the same experiment.

Further analysis of the existing data will involve a functional characterization of the identified differentially methylated genes using data mining software such as Ingenuity Pathways Analysis (IPA) to identify biological themes. Experimental follow up will also involve gene-specific confirmation of DNA methylation differences using, for example, the MassArray platform (Sequenom).

Table 1: Samples analyzed by microarray analysis for DNA methylation levels showing sample name, karyotype and maternal age. Samples analyzed in duplicate are indicated in the "Notes" column.

Uncultured				**Cultured**			
Sample Name	**Karyotype**	**Maternal Age**	**Notes**	**Sample Name**	**Karyotype**	**Maternal Age**	**Notes**
09-062	XX	39		CVS 32	XY +21	40	
09-071	XX	44		CVS 51	XX		
09-077	XY	41		CVS 59	XY		
09-106	XY	40		CVS 60-1	XY		
09-129	XY	46		CVS 65-1	XX +21	35	
09-172	XX	34		CVS 66-1	XX		
09-229	XX +21	43		CVS 69-1	XX +21	37	
09-314	XX +21	46		CVS 76-1	XY +21	43	
10-033	XY +21	42		CVS 60-2	XY		DUPLICATE
C-9	XY +21	40		CVS 65-2	XX +21	35	DUPLICATE
C-126	XY +21	41		CVS 66-2	XX		DUPLICATE
				CVS 69-2	XY +21	37	DUPLICATE
				CVS 76-2	XY +21	43	DUPLICATE

<u>The following column headings apply to both Table 2 and Table 3</u>
Norm.pval and **t21.pval**: p values that the probe is significantly methylated/unmethylated.
Norm.meth and **t21.meth***:* average methylation rate for normal and t21 samples respectively
Diff*:* difference in average methylation rate between normal and t21 samples.

<u>Table 2A</u>: Top ten CpG sites more highly methylated in all trisomy 21 samples compared to all normal samples.

norm. pval	T21. pval	norm. meth	t21. meth	Diff	Symbol	Product
0.01	0.23	0.26	0.62	0.36	HOXA9	homeobox protein A9 isoform a
0.62	0.17	0.44	0.67	0.23	WT1	Wilms tumor 1 isoform C
0.05	0.17	0.38	0.59	0.21	HOXA9	homeobox protein A9 isoform a
0.49	0.62	0.41	0.57	0.16	VCY	variable charge; Y-linked
0.50	0.49	0.43	0.58	0.16	PRKAR1B	protein kinase; cAMP-dependent; regulatory; type I; beta
0.77	0.02	0.49	0.64	0.15	ANKRD30A	ankyrin repeat domain 30A
0.00	0.57	0.37	0.52	0.15	ARPP-21	cyclic AMP-regulated phosphoprotein; 21 kD isoform 2
0.64	0.02	0.48	0.63	0.15	HCA112	hepatocellular carcinoma-associated antigen 112
0.25	0.31	0.43	0.57	0.15	SRD5A2	3-oxo-5 alpha-steroid 4-dehydrogenase 2
0.03	0.71	0.38	0.52	0.14	SLC9A2	solute carrier family 9 isoform 2

<u>Table 2B:</u> Top ten CpG sites more highly methylated in all normal samples compared to all trisomy 21samples.

norm. pval	t21. pval	norm. meth	t21. meth	Diff	Symbol	Product
0.01	0.78	0.68	0.48	0.20	NAP1L5	nucleosome assembly protein 1-like 5
0.04	0.58	0.63	0.46	0.17	TMC1	transmembrane channel-like 1
0.00	0.22	0.61	0.46	0.15	GRIP1	glutamate receptor interacting protein 1 isoform 2
0.92	0.00	0.50	0.36	0.15	GRID2	glutamate receptor; ionotropic; delta 2
0.79	0.21	0.52	0.41	0.11	CD83	CD83 antigen (activated B lymphocytes; immunoglobulin superfamily)
0.43	0.22	0.54	0.43	0.11	SNRPA	small nuclear ribonucleoprotein polypeptide A
0.22	0.03	0.54	0.43	0.11	ZNF232	zinc finger protein 232
0.26	0.22	0.55	0.44	0.11	ITGA8	integrin; alpha 8
0.05	0.30	0.56	0.47	0.10	SCN9A	sodium channel; voltage-gated; type IX; alpha
0.17	0.91	0.59	0.49	0.09	KCNH5	potassium voltage-gated channel; subfamily H; member 5 isoform 1

Figure 1: Hierarchical clustering of all samples. Samples of normal karyotype are represented by "norm". Trisomy 21 samples are represented by "TR21". Samples designated by the prefix "CVS" are from CV-derived cultured samples. All other samples are from uncultured CV.

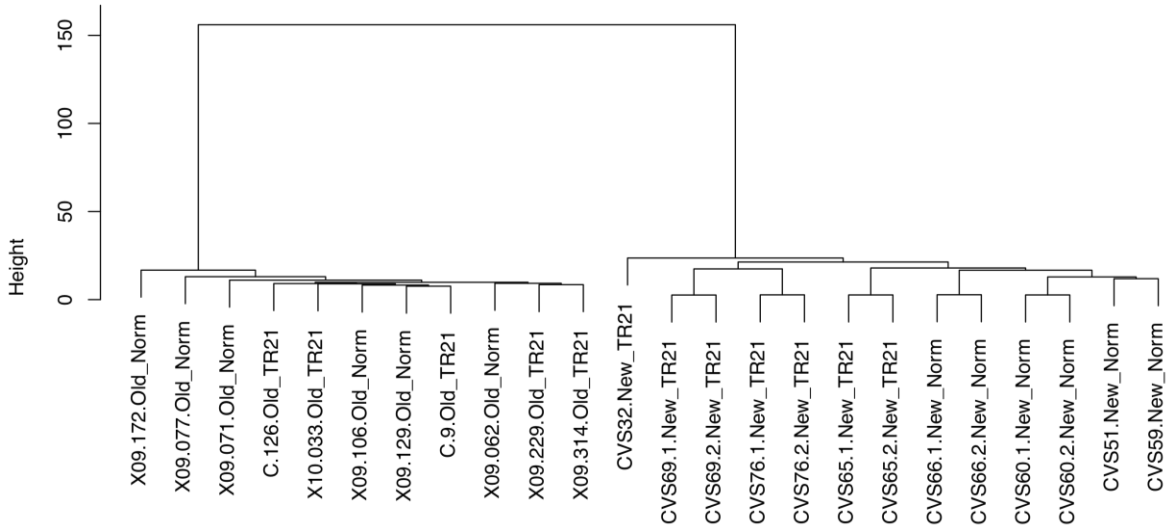

Table 3A: Top ten CpG sites more highly methylated in uncultured trisomy 21 CV samples compared to uncultured normal samples.

Norm. Pval	T21. pval	Norm. meth	T21. Meth	Diff	Symbol	Product
0.87	0.15	0.47	0.74	0.26	VCY	variable charge; Y-linked
0.86	0.00	0.49	0.74	0.25	CALN1	calneuron 1
0.02	0.00	0.40	0.65	0.25	CYP3A4	cytochrome P450; subfamily IIIA; polypeptide 4
0.09	0.05	0.40	0.63	0.24	FAM47B	hypothetical protein LOC170062
0.00	0.76	0.28	0.52	0.23	CRH	corticotropin releasing hormone precursor
0.03	0.54	0.33	0.55	0.22	HOXA9	homeobox protein A9 isoform a
0.01	0.27	0.35	0.56	0.22	ATP1B4	ATPase; (Na+)/K+ transporting; beta 4 polypeptide
0.00	0.02	0.38	0.59	0.21	PRPS1L1	phosphoribosyl pyrophosphate synthetase 1-like 1
0.00	0.73	0.31	0.52	0.21	GPR32	G protein-coupled receptor 32
0.00	0.23	0.35	0.55	0.20	PPM1G	protein phosphatase 1G

Table 3B: Top ten CpG sites more highly methylated in uncultured normal CV samples compared to uncultured trisomy 21 CV samples.

Norm. Pval	T21. pval	Norm. meth	T21. meth	Diff	Symbol	Product
0.05	0.16	0.67	0.37	0.30	NAP1L5	nucleosome assembly protein 1-like 5
0.11	0.32	0.61	0.42	0.19	HTRA4	HtrA serine peptidase 4
0.00	0.01	0.60	0.42	0.18	RPH3A	rabphilin 3A homolog
0.23	0.00	0.55	0.37	0.18	FLJ10916	hypothetical protein LOC55258
0.00	0.53	0.65	0.47	0.17	GRIP1	glutamate receptor interacting protein 1 isoform 2
0.92	0.06	0.51	0.35	0.16	TDG	thymine-DNA glycosylase isoform 2
0.20	0.32	0.58	0.43	0.15	GPR62	G protein-coupled receptor 62
0.22	0.17	0.56	0.42	0.14	SH3BP2	SH3-domain binding protein 2
0.83	0.02	0.51	0.37	0.14	ITGA8	integrin; alpha 8
0.02	0.29	0.59	0.46	0.13	SKIV2L	superkiller viralicidic activity 2-like homolog

Table 3C: Top ten CpG sites more highly methylated in cultured trisomy 21 CV-derived samples compared to cultured normal CV-derived samples.

Norm. Pval	T21. pval	Norm. meth	T21. meth	Diff	Symbol	Product
1.58E-05	0.01	0.24	0.65	0.41	SEC31L2	S. cerevisiae SEC31-like 2 isoform a
0.49	0.04	0.41	0.79	0.38	HOXA9	homeobox protein A9 isoform a
0.09	0.74	0.20	0.58	0.38	CYP2E1	cytochrome P450; family 2; subfamily E; polypeptide 1
0.01	0.31	0.24	0.62	0.37	NOL3	nucleolar protein 3
0.00	0.67	0.18	0.52	0.34	PNMA2	paraneoplastic antigen MA2
0.00	0.21	0.26	0.59	0.33	VIPR2	vasoactive intestinal peptide receptor 2
0.00	0.90	0.19	0.52	0.32	FAM3B	family with sequence similarity 3; member B isoform a
0.30	0.07	0.39	0.71	0.32	NKX6-2	NK6 transcription factor related; locus 2
0.00	0.22	0.27	0.58	0.32	HIST1H3E	H3 histone family; member D
0.00	0.35	0.27	0.58	0.31	HOXA9	homeobox protein A9 isoform a

Table 3D: Top ten CpG sites more highly methylated in cultured normal CV-derived samples compared to cultured trisomy CV-derived samples.

Norm. Pval	T21. pval	Norm. meth	T21. Meth	Diff	Symbol	Product
0.47	0.00	0.53	0.29	0.25	HTR3D	5-hydroxytryptamine receptor 3 subunit D
0.33	0.02	0.56	0.32	0.25	CSPG3	chondroitin sulfate proteoglycan 3 (neurocan)
0.01	0.28	0.66	0.43	0.22	C10orf39	hypothetical protein LOC282973
0.00	0.95	0.72	0.50	0.22	LILRB4	leukocyte immunoglobulin-like receptor; subfamily B (with TM and ITIM domains); member 4
0.23	0.57	0.64	0.42	0.22	TRPC5	transient receptor potential cation channel; subfamily C; member 5
0.96	0.00	0.50	0.29	0.21	BAK1	BCL2-antagonist/killer 1
0.66	0.00	0.52	0.31	0.21	LOC348645	hypothetical protein LOC348645
0.01	0.00	0.59	0.39	0.20	CEACAM3	carcinoembryonic antigen-related cell adhesion molecule 3
0.19	0.35	0.60	0.41	0.19	MAGEA1	melanoma antigen family A; 1
0.16	0.01	0.55	0.37	0.18	XCL2	chemokine (C motif) ligand 2

Research Project 6: Project Title and Purpose

Antigen Expression and Adaptive Immunity in Human Endometriosis and Endometriosis-Related Ovarian Cancers - Ovarian cancer most often presents as advanced disease and survival at 5 years is very low. We postulate that identification of precursor lesions would allow for timely detection of early ovarian cancer and will ultimately improve survival. To date, the only precursor lesion reported in ovarian cancer is endometriosis, a common disease which can affect up to 10% of reproductive-age women. However, the major pathogenesis mechanisms are not well understood in either ovarian cancer or endometriosis. One common denominator of these two clinical entities is chronic inflammation, given by the interaction of cancer cell-intrinsic factors and the host immune system. We postulate that a better understanding of the role of the adaptive immune system in endometriosis could potentially contribute to the design of vaccines used for ovarian cancer prevention rather than therapy.

Anticipated Duration of Project

1/1/2010 - 12/31/2010

Project Overview

An intact immune system is capable of surveying for cancerous or even precancerous lesions and eradicating them before they become clinically significant. This process is known as immunosurveillance and relies on the function of highly specialized immune cells and their secreted molecules (called adaptive immunity). The immune mechanisms (and their failures) although studied in cancer, are much less understood in premalignancy, including endometriosis. We postulate that in the context of chronic inflammation, the immune surveillance may in fact contribute toward lesion development (invasion, angiogenesis etc) and malignant transformation. We propose here to characterize the interactions between the epithelial cells and immune cells in the microenvironment, in endometriosis and ovarian cancer. Some of these interactions are antigen-specific, in response to protein antigens expressed by the epithelial cells during disease progression. One such antigen is MUC1, a well known oncoprotein and tumor-associated antigen widely expressed in all types of ovarian tumors and present in endometriosis. Our previous studies in MUC1 Tg mice with conditional Kras mutations (MUC1Kras mice) progressing to endometriosis-like lesions illustrate a progressive increasing in MUC1 expression and T cell dysfunction suggestive of Th2/Treg bias. Ovarian tumor-bearing (MUC1KrasPTEN) triple transgenic mice also show presence of Th17 cells in advanced disease. Based on these results, we propose here the following aims:

Specific Aim 1: To identify the mechanisms of immune surveillance in peripheral blood and lesion microenvironment in human endometriosis and ovarian cancer. We will explore T and B-cell mediated immunity and characterize the immune balance between CD4+ T cell subsets, specifically Treg and Th17 subsets, in human endometriotic lesions. As controls we will use patients with malignancy (cancer control patients) and patients with benign lesions (physiologic cysts- benign control patients). We will use several platforms to profile antigen expression and immunity, using immunohistochemistry, flow cytometry and quantitative real time PCR arrays.

Specific Aim 2: To identify MUC1 roles in ovarian carcinogenesis. For this aim we will use 2 categories of transgenic mice, both progressing to de novo ovarian tumors: 1. triple transgenic (Tg) MUC1KrasPTEN mice which develop human MUC1-expressing ovarian tumors and 2. double Tg KrasPTEN mice, which develop MUC1-negative ovarian tumors. These mice will allow us to characterize phenotypic differences due to human MUC1 and identify potential new therapeutic targets.

Principal Investigator

Anda M Vlad, MD, PhD
Assistant Professor
University of Pittsburgh
Magee Women's Research Institute
204 Craft Ave., B403
Pittsburgh PA 15213

Other Participating Researchers

Raluca Budiu, PhD - employed by University of Pittsburgh
Joan Brozick, BS - employed by University of Pittsburgh Medical Center

Expected Research Outcomes and Benefits

Immediate significance: Our studies will further our understanding on the role of the immune system in disease pathogenesis in endometriosis and it will provide insight on the expression of MUC1 antigen in endometriosis.

Long-term impact: Results from these studies will hopefully provide the basis for the next generation MUC1 vaccines and immune biologics, targeting prevention rather than cancer treatment.

Many clinicians and translational scientists currently allocate substantial efforts to the design and implementation of vaccines and immune biologics as adjuvant therapy in late stage cancer patients. Most often, the patients are terminally ill, and the disease is resistant to standard therapy. Not surprisingly, the immune system in these patients is exhausted and unable to respond to its full potential given the disease burden. On the other hand, however, patients with long-lasting, chronic premalignant disease (like endometriosis) are generally younger and better candidates for vaccines or immune biologics. Studies presented here will hopefully provide a first step toward the design of preventive vaccines.

Summary of Research Completed

During the reporting period the PI has made significant progress on the specific aims. Details of our preliminary task achievements are described below.

Specific Aim 1: To identify the mechanisms of immune surveillance in peripheral blood and lesion microenvironment in human endometriosis and ovarian cancer.

Our hypothesis is that adaptive immune cells, particularly T cells and their secreted factors could functionally contribute toward lesion development (i.e., invasion, oxygenation, angiogenesis etc) in endometriosis and may potentially drive ovarian carcinogenesis. To test this hypothesis, we proposed to explore T cell immunity and characterize the immune balance between CD4+ T cell subsets using immunohistochemistry, flow cytometry and quantitative real time PCR arrays.

Specimen accrual.
During the reporting period we have completed the accrual of all specimens, as planned:
n=20 ovarian endometriotic lesions and associated fluids, n=15 endometriosis-related cancers (tissue biopsies, blood, ascites etc) and n=15 normal controls (tissue, peripheral blood).
The specimens were obtained from the Health Science Tissue Bank at Magee-Women's Hospital and the Gynecologic Specimen Bank, according to approved IRB protocols.
The peripheral blood mononuclear cells (PBMCs) and plasma were separated and cryopreserved until ready to use.
All tissue biopsies were processed for formalin fixation and paraffin embedding.

RNA extraction and qRT-PCR arrays.
We have completed the RNA extraction from all PBMC and tissue sections (from all 3 patient categories: endometriosis, ovarian cancer and normal controls).
The PBMC- and tissue extracted RNA was subjected to the Th1-Th2-Th3 PCR array (SABiosciences), described in the research plan. The arrays were run in 384-well plates, using the 7900HT Fast Real-Time PCR System with 384-Well Block Module (Applied Biosystems) housed at MWRI's molecular core facility. All data sets are currently analyzed for statistical significance.

Immunohistochemistry.
We stained all tissue biopsies with antibodies for MUC1 tumor-associated antigen and for T cell markers (CD3, CD4, CD8, FOXP3) to identify the makeup of immune infiltrates in the lesion microenvironment. Examples of the staining pattern observed are shown in Figures 1 and 2.
Our preliminary analysis shows that ectopic endometriotic glands maintain MUC1 expression (Fig. 1). Nevertheless, the protein expression level and distribution pattern (membranous and cytosolic) is different from that on eutopic glands, where MUC1 is generally discrete and polarized to the apical membranes (Fig. 1).Immune cells, including CD3, CD4, Treg, and CD8 T cells, are present in endometriotic lesions and appear to be more abundant than in eutopic glands (Fig. 2 and data not shown).
All quantifications are currently reviewed by a pathologist with expertise in gynecologic diseases.

MUC1-specific antibody measurements.
All blood specimens have been processed for plasma separation and have been cryopreserved for antibody measurement by ELISA, soon to be performed.

Specific Aim 2: To identify MUC1 roles in ovarian carcinogenesis.

Evidence from tumors of the pancreas, breast and colon suggests that MUC1 glycoprotein acts as an oncogene and may participate in carcinogenesis. We hypothesize here that MUC1 may also participate in ovarian carcinogenesis. To test this we proposed to use two sets of genetically engineered (transgenic, Tg) mice: double Tg KrasPTEN mice and triple Tg MUC1KrasPTEN mice. Both mouse sets progress to de novo ovarian tumors, with a phenotype similar to the human disease. However, the tumors in triple Tg mice express the human MUC1 antigen while the tumors in the double Tg mice are MUC1 negative.

Survival surgery and tumor induction via AdCre intrabursal administration
Given the relatively low incidence of mice with the triple transgenic phenotype, we have set up numerous mouse breeding colonies and carried on a large mouse breeding program, as originally planned. All littermates were genotyped by PCR and the mice (identified with either the triple or double transgenic (Tg) genotype, MUC1KrasPten and KrasPten, respectively) were included in the experimental group. The experimental animals were subjected to survival surgery and injected with 5 μl of 2.5 x 10^7 plaque forming units (p.f.u.) of AdCre/mouse in the bursa of only one of the ovaries (keeping the contralateral as negative control).

We have so far completed ovarian cancer induction in 7 triple Tg mice.
We have observed that the ovarian tumors progress faster in triple Tg mice, are more likely to spread throughout the peritoneal cavity (carcinomatosis) and to be accompanied by hemorrhagic ascites. Our interim analysis shows that the survival time in triple Tg mice (average of 6 weeks) is significantly shorter than in double Tg (average of 11 weeks), suggesting a more aggressive tumor behavior due to the human MUC1 transgene. The survival analysis is currently being finalized.

Histology assessment of tumor antigen expression.
We sacrificed the tumor bearing mice and harvested at necropsy the tumors and lymphoid organs, as originally proposed.
The tumors were formalin fixed and paraffin embedded for immunohistochemistry (IHC).
We have so far performed IHC staining for MUC1 (human) (Fig. 3) and Muc1 (mouse) antigen (not shown) expression, using specific antibodies.
For human MUC1 expression we used an antibody (clone HMFG) specific for a human epitope within MUC1 extracellular domain. As expected, this antibody detects MUC1 expression in triple Tg mice only (Fig. 3B). We also used an antibody (CT2) specific for an epitope within the cytosolic domain (CD). Since this epitope is present in both, the human as well as the mouse mucin 1 CD, positive staining with CT2 would be therefore indicative of both mouse and human mucin 1 presence.
Our analysis revealed that in healthy triple Tg mice the normal ovarian surface epithelium (OSE) stain positive for HMFG and CT2, while the double Tg mice stain negative for both, suggestive of human and not mouse mucin1 presence on OSE (not shown).
The ovarian tumors from triple Tg mice, stain highly positive for MUC1 and positive for CT2 (not shown). In contrast the tumors from double Tg mice stain negative for CT2 (Fig. 3A and B), reemphasizing the idea that MUC1, but not Muc1, is highly present on OSE-derived tumors.

These results point out to MUC1-specific role in ovarian cancer which will be further addressed in the second half of this funding period. .

Immune monitoring.
We processed the para-aortic lymph nodes and spleens from all double and triple Tg tumor-bearing mice into single cell suspensions for flow cytometry phenotyping and compared Treg accumulation in triple Tg and double Tg mice.
So far we focused primarily on the two major subtypes of T cells, CD4 + T helper lymphocytes and cytotoxic CD8 T cells in the spleens of tumor-bearing mice, by flow cytometry. Our interim analysis, suggests a dramatic decrease in CD3 positive T cells and a change in the ratio of CD4/CD8 T cells in the triple Tg mice compared with double tg mice. These findings were also reflected in the IHC staining of the spleens, showing significant changes in the organ architecture (Fig. 4) of spleens from the triple Tg animals. Further analysis of the cohort will establish the statistical significance of theses interim differences.

In summary, our experiments have successfully progressed and the milestones have been reached, according to our original plan.

Figures

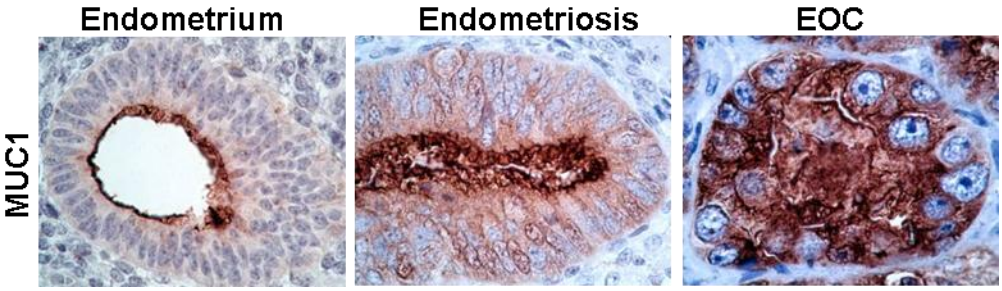

Fig. 1. MUC1 expression in eutopic endometrial glands (left panel), ectopic endometriotic glands (middle panel) and in epithelial ovarian cancer (EOC, right panel). Immunohistochemistry (IHC) was performed on formalin-fixed paraffin-embedded tissue (FFPE), using a monoclonal antibody to human MUC1 (clone HMFG,1:500 dilution). MUC1 presence is illustrated by brown staining. MUC1 is membranous and polarized on the apical surface of normal, eutopic endometrial glands, facing the ductal lumen (left). In ectopic glands (middle), MUC1 seems overexpressed. In addition to being luminal, there is also increased cytosolic MUC1 expression. The right panel shows extremely high MUC1 expression in endometrioid ovarian cancer.

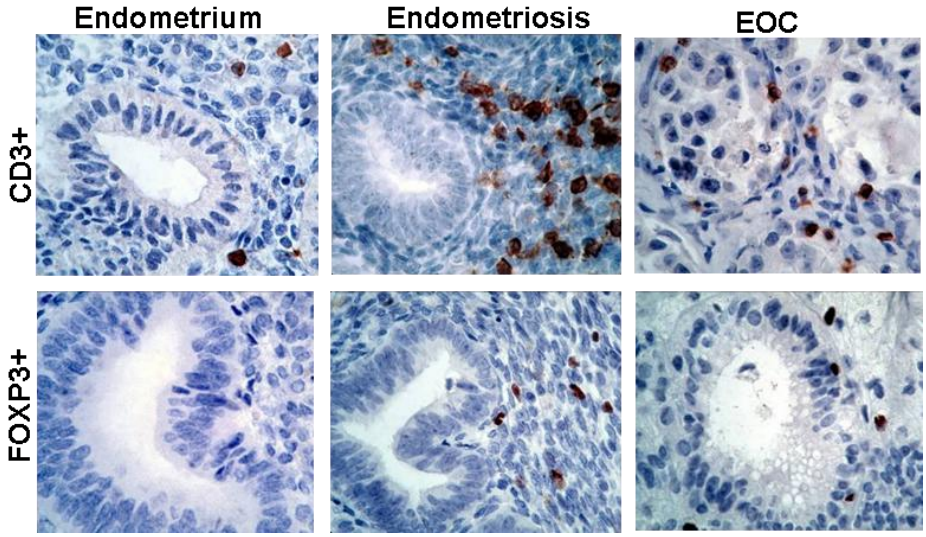

Fig. 2. Detection of immune cell infiltrates in the endometrium (left panels), endometriosis stroma (middle) and epithelial ovarian tumors (right panels). Immunohistochemistry (IHC) was performed on formalin-fixed paraffin-embedded tissue (FFPE), using monoclonal antibodies to human CD3 (upper panels) or FOXP3 (lower panels). CD3 is a pan-T cell marker while FOXP3 is a transcription factor expressed in regulatory immune suppressive CD4 T cells (Tregs).

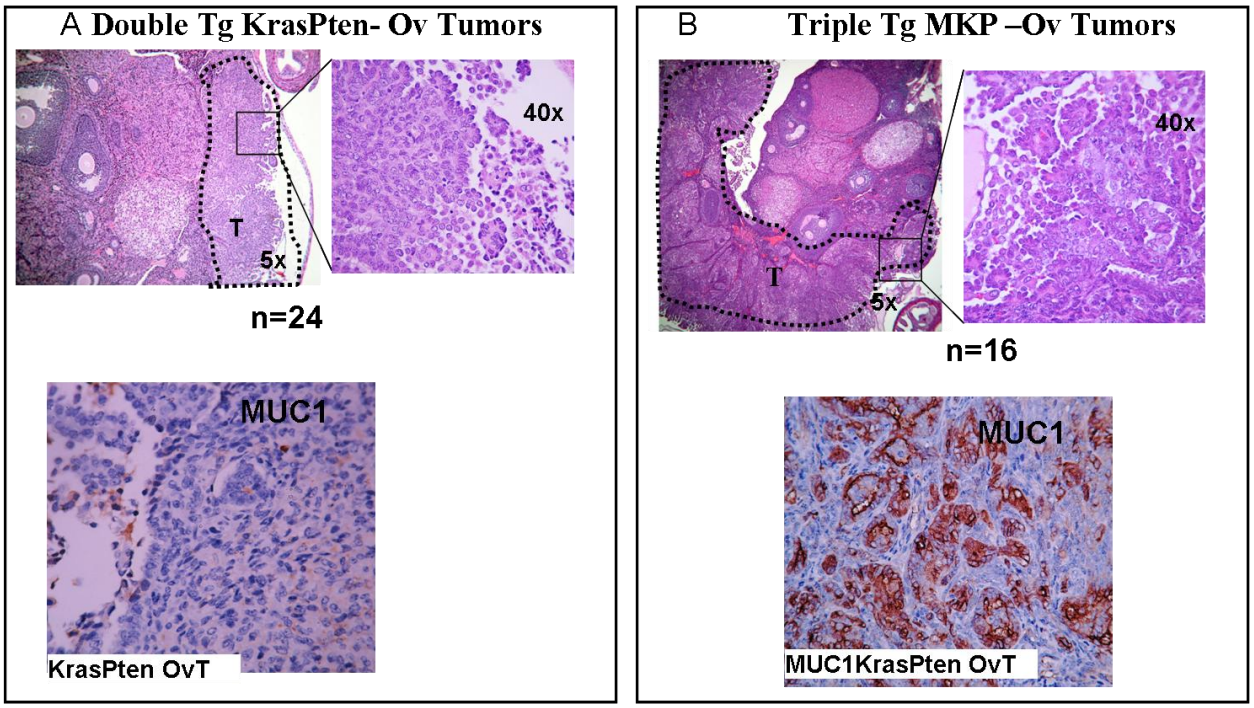

Fig. 3. Triple Tg mice $MUC1^{+/-}Kras^{G12D/+}Pten^{loxP/loxP}$ mice develop MUC1 + ovarian tumors. The tumors in both double (Fig. 3A) and triple (Fig. 3B) Tg mice develop in the injected ovary only (dotted lines) and have similar histology, consistent with a papillary clear cell carcinoma. In contrast to the tumors in double Tg mice (bottom left) only the triple Tg tumors (bottom right) express MUC1. IHC was performed with the MUC1-specific antibody (clone HMFG, as described above).

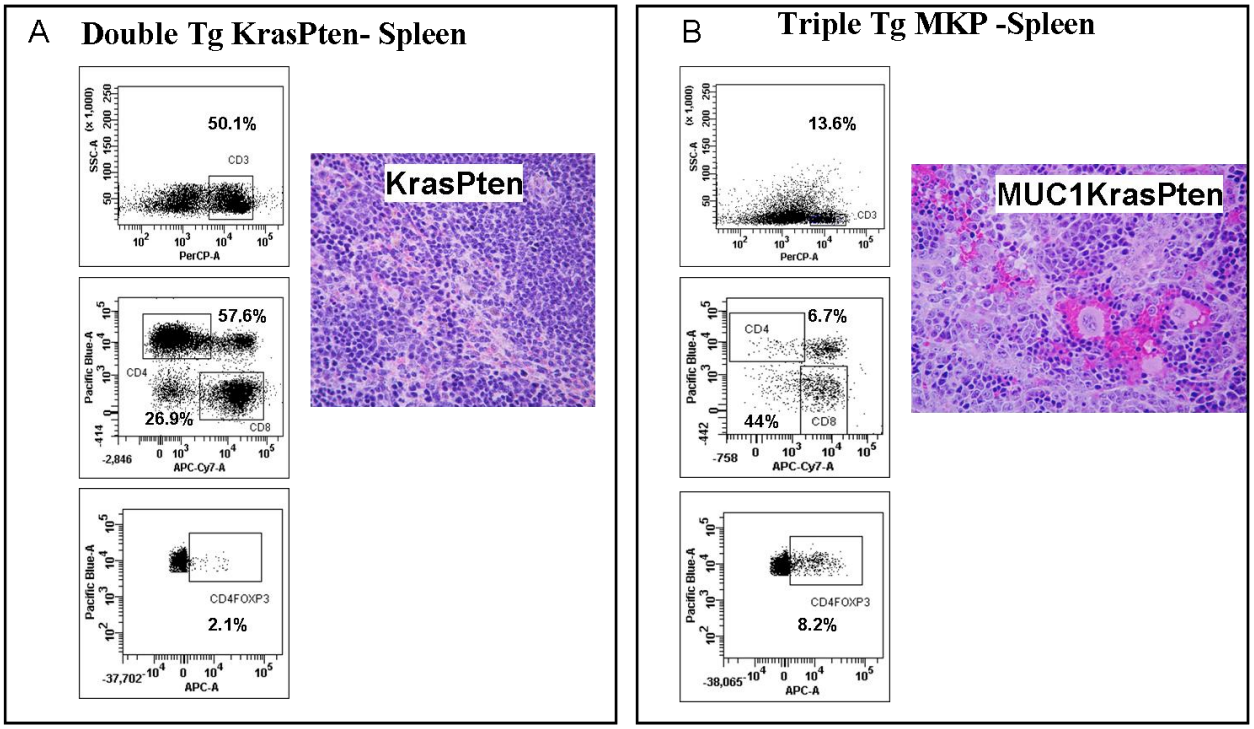

Fig. 4. Major differences in the cellular composition of spleens in double (Fig. 4A) versus triple Tg mice (Fig. 4B) with tumors. Flow cytometry (dot plots) in triple Tg mice show dramatically decreased percentages in CD3 T cells (upper dot plots), inversed CD4/CD8 ratio (middle dot plots) and increased accumulation of Tregs (lower dot plots). The spleen histology also increased angiogenesis and abnormal architecture in triple Tg mice.

<u>Research Project 7: Project Title and Purpose</u>

The Impact of Age on the Nematode Germline - In human oocytes, defects in meiotic crossover exchanges are the most significant age related abnormality. Nevertheless, our understanding of the processes that control where and how many crossovers occur is not well understood. Furthermore, it is unclear how aging impinges on different crossover configurations to increase missegregation at increased maternal age. Our studies in the nematode *C. elegans* will use high resolution confocal imaging to identify changes in the germline chromatin structure during normal aging and will analyze how aging pathways influence these processes. These studies have the potential to identify genes and pathways that lead human aneuploidy and therefore may identify targets for therapeutic purposes.

Anticipated Duration of Project

1/1/2010 - 12/31/2010

Project Overview

The goal of this research is to identify factors contributing to the age-related decline in fertility and the associated increase in trisomies. As women age, oocytes show problems in meiosis that lead to chromosomal nondisjunction (NDJ), including Turner and Down Syndromes. The majority of NDJ is due to defects in meiotic crossover recombination (CO). A growing body of literature places chromatin structure as a key determinant of CO formation. Thus changes in germline chromatin impact embryonic outcomes and through epigenetic inheritance, chromatin affects offspring fecundity. We will study age-related changes in germline chromatin in the model genetic system, the nematode *C. elegans* because there is strong conservation in aging pathways and in the meiotic process between worm and humans.

1) Characterize changes in germline chromatin during normal aging. Histone post-translational modifications and histone variant influence gene activity, DNA damage repair, and meiotic recombination and thus play a critical role in genome integrity. Because environment and age can modulate chromatin structure, we hypothesize that age-dependent changes in chromatin structure increase NDJ and predispose progeny to reproductive problems. We will characterize histone post-translational modifications and histone variants in the germlines of young and aged animals using immunofluorescence and high-resolution confocal imaging. These studies have the potential of precisely describing how chromatin changes in the germline of aging animals and thus may reveal targets for reproductive therapies.

2) Identify molecular pathways controlling age-related changes in germline chromatin. Changes in chromatin structure are mediated by the histone modifying enzymes that catalyze the addition and removal of these marks. Chromatin structure is also influenced by endocrine signaling and environment which affect the expression and activity of these enzymes. In this aim, we will identify changes in expression of histone modifying enzymes during germline aging and associate these changes with specific modifications. We will also determine which of the aging pathways impinge on germline chromatin, by monitoring histone post-translational modifications and histone variants in longevity mutants. Initial efforts will focus on the characterization of *sir-2*, which has a direct role in chromatin modification and aging, and the insulin/IGF-1 signaling pathway, which affects resistance to germline tumors and reduces fecundity.

Principal Investigator

Judith L. Yanowitz, PhD
Assistant Professor
Magee-Womens Research Institute
204 Craft Ave, B705
Pittsburgh PA 15213

Other Participating Researchers

None

Expected Research Outcomes and Benefits

The ultimate goal of this work is to find conserved molecular pathways that inform our understanding of human infertility. Defining the genetic mechanisms that underlie defects in meiotic recombination and subsequent chromosome segregation is a critical step for understanding human reproductive aging. Chromatin organization is a major determinant of crossover regulation, influencing where and how many crossovers occur. Sex, age and temperature strongly influence the placement of crossovers along the chromosome by shifting the usage of chromosomal domains leading to the hypothesis that these factors influence crossover formation by altering germline chromatin. Our studies should identify specific histone post-translational modifications that are altered in aging animals and the aging pathways that are responsible for such changes. These findings have immediate applications for fertility research because drugs targeting either specific histone modifying enzymes and aging pathway components can be tested for their immediate effect on reproductive outcomes in the nematode. These results can then be used to inform studies in mammals, and ultimately the clinic. A second, potential outcome of these studies is the identification of potential targets for environmental toxicants within the germline. Aging pathways and stress pathways are intimately linked and many environmental toxins activate these pathways. Therefore, a greater understanding of germline targets of aging can inform our understanding of how stress and toxins act within the germline. The recent realization that bisphenol A, a commonly used plasticizer, has severe germline phenotypes over multiple generations underscores the importance of our studies.

Summary of Research Completed

We have been analyzing histone post-translational modifications in the germlines of aging worms in order to determine if changes in chromatin structure contribute to reproductive decline and aneuploidy. Our initial goal was to examine histone post-translational modifications (HPTMs) in day 1, 5 and 9 adult germlines of the nematode, *C. elegans*, as these days correspond to the initiation of egg-laying, the onset of reproductive decline and reproductive senescence, respectively.

One major concern in these experiments was the ability to isolate and fix older animals. In the only published study that looked at aged germline tissues, only whole mount DNA staining was performed. That study found significant changes in germline morphology, including disorganization and accumulation of yolk. Therefore, we initiated our studies by optimizing protocols for fixation of aged gonads. We found that older animals were more fragile than younger in laboratory manipulations and were generally more difficult to dissect. Therefore a greater number of animals were required at the outset to attain sufficient numbers of animals for analysis. However, we found that once dissected, the aged tissue was equally amenable to paraformaldehyde, ethanol, and methanol/acetone fixation protocols and posed no difficulties compared to adult day 1 tissue.

During the course of these experiments, we generated a large number of tissue samples of young and old germlines that we used to characterize age-related changes during reproductive aging, based simply on germ cell structure or organization. These studies have revealed that aging in the

germline, as in the soma, is stochastic, with some animals having acute defects and others quite mild defect as compared to young adults. The spectrum of defects observed included decreased numbers of germline nuclei, disorganization in the spatial or temporal organization of germ cells, increases in the number of non-recombinant chromosomes (which leads to aneuploidy), DNA fusions and endoreduplication (Figure 1). This work lays the foundation for the rest of the planned studies in this grant by defining the processes that may be most age-sensitive and therefore most likely affected by changes in germline chromatin.

Having established protocols for fixation and analysis of aged germline tissues, we have begun to examine HPTMs in these animals. All samples were to be analyzed on a Nikon A1r confocal microscope purchased with funds provided by this grant. Set-up of the confocal system was delayed until late June due to required modifications to the microscope facility that houses the confocal, as well as to technical difficulties that arose during building and testing. This system is now fully functional and able to attain high quality images of HPTMs in germ cell nuclei (see for example, Figure 2).

We have efficiently labeled young and aged adult germ cells with eleven HPTM-specific antibodies (Table 1). Using a fluorescent, widefield microscope and deconvolution software, we have been able to analyze the global distributions of these HPTMs. In the majority of cases, we saw no difference in HPTM distribution in young versus old adult germline tissue. In several cases, our preliminary analyses indicate changes in staining intensity as compared to wild type, as indicated in Table 1. Surprisingly, we have not yet observed any drastic changes in overall localization of HPTMs, suggesting that the profound decrease in reproductive potential and outcomes with age, are not due to an all-or-none effects of a single HPTM. Instead, the subtle changes in HPTM staining may suggest that age-related defects result from the cumulative effect of minor changes in multiple pathways. Alternatively, the observation that aging varies between individuals (described above) may suggest that more dramatic changes in chromatin architecture may be limited to a subset of animals in the population. Extending the current work to a greater number of animals as well as to the sub-nuclear distribution of each HPTM will likely resolve these issues and have potential to highlight specific modifications with more significant roles. One caveat to these interpretations is that our analysis is limited to only a subset of the total HPTMs; an as yet uncharacterized modification could serve as a *bona fide* rheostat for age in the germline.

We also proposed to analyze the expression and localization of histone variants. Histone variants influence chromatin organization and often confer unique functions. GFP-tagged transgenes are available for a number of the variants and allow us to directly monitor protein localization without fixation. We have attained transgenes for histone H1, H2 and H3 variants and are preparing animals for analysis.

In aim 2, we proposed to determine whether somatic aging pathways function in germline aging and HPTM-associated changes. As a first step in this process, we have analyzed mutants defective in either of two Sir2 homologs, *sir-2.1* or *sir-2.3*, or the insulin-like receptor, *daf-2*, to determine whether influence reproductive lifespan of the animals. Animals were mated at day 1, 2 and then transferred every day to fresh plates until 48 hours post- egg laying. Total numbers of progeny and reproductive span were determined by counting progeny each day. Although these

mutants have been implicated in germline function, no change in the reproductive span was observed in our studies and all animals had ceased egg-laying by day 9. Thus it appears that *sir-2.1*, *sir-2.3* and *daf-2* are not required for reproductive senescence. These strains are being further analyzed to determine whether nondisjunction and meiotic progression are affected in these mutant backgrounds.

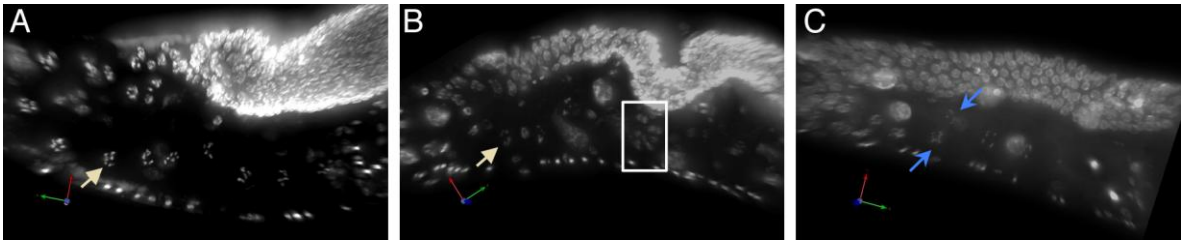

Figure 1. Analysis of changes in aging germlines. (A) DAPI stained imaged of the proximal gonad from adult day 1 *C. elegans*. Yellow arrow marks on of the diakinesis oocytes with 6 bivalents, corresponding to the 6 pairs of homologues that are held together at the site of crossing over. Note the extended line of diakinesis oocytes in the young samples. (B, C) Day 9 gonads. (B) Yellow arrow again marks a normal oocytes with 6 foci; the white box demarcates a population of nuclei that are displaced from the pachytene region and interspersed with diakinesis oocytes. (C) Blue arrows point to several nuclei with greater than 6 foci, indicating several chromosomes that have not received crossovers and may missegregate upon cell division. In day 9 samples, note the dearth of diakinesis oocytes.

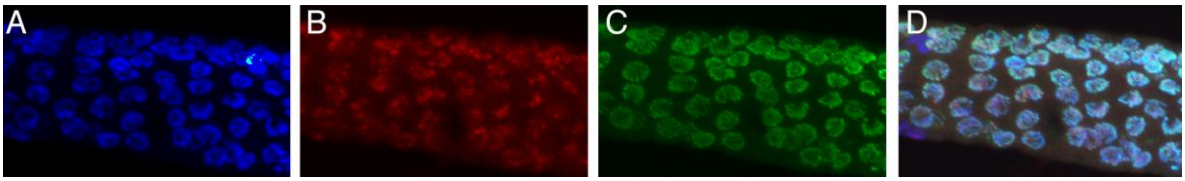

Figure 2. Adult day 1 gonads stained with DAPI (A), anti-H2A acetylated lysine 5 (B), anti- Htp-1, a chromosome axis protein (C), and an overlay of all three images (D). Germ cells were imaged on the Nikon A1r confocal system.

Table 1. Histone Post-Translation Modifications Analyzed

Antibody	Company	Staining[a]		Antibody	Company	Staining
H2A K5Ac	Cell Signaling	Yes		H2A K5Ac	Upstate	Decrease
H3K4me2	Upstate	Increased		H4K5Ac	Millipore	Yes
H3K4me3	Lake Placid	Yes		H4K8Ac	Abcam	Yes
H3K9me2	Upstate	Yes (Weak)		H4K12Ac	Abcam	Yes
H3K9me3	Abcam	Yes		H4K16Ac	Upstate	Yes
H3K9Ac	Cell Signaling	Decreased				

[a]Yes indicates that staining was observed with no differences between wild type and mutant; increased and decreased are a measure of adult day 9 staining compared to adult day 1.